Pergamon

0013-7944(95)00018-6

Engineering Fracture Mechanics Vol. 52, No. 2, pp. 265–288, 1995

0013-7944/95 $9.50 + 0.00

A STOCHASTIC MODEL FOR ELASTIC–PLASTIC FRACTURE ANALYSIS OF CIRCUMFERENTIAL THROUGH-WALL-CRACKED PIPES SUBJECT TO BENDING

SHARIF RAHMAN

Engineering Mechanics Department, Battelle Memorial Institute, Columbus, OH 43201, U.S.A.

Abstract—A probabilistic model is developed for nonlinear fracture-mechanics analysis of through-walled-cracked pipes subject to bending loads. It involves elastic–plastic finite element analysis for estimating energy release rates, J-tearing theory for characterizing ductile fracture and standard structural reliability methods for conducting probabilistic analysis. Evaluation of the J-integral is based on the deformation theory of plasticity and power-law idealizations of stress–strain and fracture toughness curves. This allows the J-integral to be expressed in terms of non-dimensional influence functions (F- and h_1-functions) that depend on crack size, pipe geometry and material hardening constant. The equations for these functions (and hence, J) for a cracked pipe are developed in closed-form based on recent results of elastic–plastic finite element analysis. This makes the subsequent stochastic analysis computationally feasible to conduct probabilistic pipe fracture evaluations. Both analytical and simulation methods are formulated to determine probabilistic characteristics of J for a circumferential through-wall-cracked pipe as a function of applied bending moment. The same methods are used later to compute failure probability of the cracked pipes. Several failure criteria associated with crack initiation, unstable crack growth and Net-Section-Collapse are used to determine such probabilities.

Numerical applications are provided to illustrate the proposed methodology. First, the validity of the J-integral based on the proposed equations for predicting the crack driving force in a through-wall-cracked pipe is evaluated by comparing with available results in the current literature. Second, probability densities of the J-integral are predicted as a function of applied loads. Third, failure probabilities corresponding to various performance criteria are evaluated for a stainless steel nuclear piping in the Boiling Water Reactor plant. The effects of correlation and distribution properties of random input on failure probability are also evaluated.

1. INTRODUCTION

STRUCTURAL COMPONENTS, which are comprised of piping systems, can be found in nuclear power plants, off-shore drilling platforms, fossil power generation plants, gas pipelines and others. The unavoidable existence of cracks in some components may lead to increased safety concerns about the loss of structural strength and possibly failure of these structural systems. Traditional approach to safety assessment and design lies in a deterministic model which invariably involves a large safety factor usually assigned from heuristic and somewhat arbitrary decisions. This approach has almost certainly been reinforced by the very large extent to which structural engineering design is codified and the lack of feedback about the actual performance of the structure. Use of large safety factors can lead to the view that "absolute" safety can be achieved. Absolute safety is, of course, undesirable if not unobtainable, since it could only be approached by deploying infinite resources. Moreover, these safety factors do not provide any information regarding the probability that a pre-existing flaw would lead to the loss of the pipe's structural integrity.

A realistic evaluation of structural performance can be conducted only if the uncertainty in structural loads, flaw sizes and material properties, and hence responses, are taken into consideration. Typical response parameters of piping systems that undergo plastic deformation due to applied loads are the J-integral, crack-tip opening displacement and others. While the load and the resistance are not deterministic, they nevertheless show statistical regularity and the statistical information, which is necessary to describe their probability laws, is available from the existing literature, e.g. the material properties of base and weld metals used in typical nuclear piping can be obtained from the PIFRAC database [1], the Degraded Piping Program [2] and the International Piping Integrity Research Group (IPIRG) Program [3] and others [4–6]. A diligent search of the above database from these research programs can provide a wealth of data for statistical characterization of the strength (stress–strain curve) and the toughness (J-resistance) properties of

typical pipe materials. These suggest that the probability theory and structural reliability methods can be applied to assess performance of piping and piping welds subjected to in-service (normal operational loads) and extreme (seismic loads) loading environments.

The objective of this paper is to develop a probabilistic model for nonlinear fracture-mechanics analysis of circumferential through-walled-cracked (TWC) pipes subject to bending loads. It involves (1) elastic–plastic finite-element analysis for estimating energy release rates, (2) J-tearing theory for characterizing ductile fracture and (3) standard methods of structural reliability theory for conducting probabilistic analysis. The evaluation of the J-integral is based on the deformation theory of plasticity and constitutive law characterized by the power-law equation for the stress–strain curve. This permits the J-integral to be expressed in terms of non-dimensional influence functions that depend on crack geometry, pipe geometry and material hardening constant. The equations for these functions (and hence, J) for a cracked pipe are developed in closed-form based on recent results of elastic–plastic finite element analysis. This makes the subsequent stochastic analysis computationally feasible to evaluate probabilistic characteristics of the J-integral and failure loads. Both analytical and computational methods (e.g. First- and Second-Order Reliability Methods) and simulation methods (e.g. Monte Carlo Simulation and Importance Sampling) are formulated to determine relevant probability measures for pipe fracture evaluations. Numerical examples are presented to illustrate the proposed methodology.

2. ELASTIC–PLASTIC FRACTURE ANALYSIS OF TWC PIPES

It is now well-established that the elastic–plastic fracture mechanics (EPFM) provide more realistic measures of fracture behavior of cracked engineering systems when compared with the elastic methods. The use of EPFM becomes almost necessary for structural materials with high toughness and low strength, which generally undergo extensive plastic deformation around a crack tip. Recent analytical, experimental and computational studies on this subject indicate that the energy release rate (also known as J-integral) and crack-tip opening displacement (CTOD) are the most viable fracture parameters for characterizing crack initiation, stable crack growth and subsequent instability in ductile materials [7, 8]. This clearly suggests that the global parameters like J and/or CTOD can be conveniently used to assess structural integrity for both leak-before-break and in-service flaw acceptance criteria in degraded piping systems. It is, however, noted that the parameter J still possesses some theoretical limitations, e.g. the Hutchinson–Rice–Rosengren (HRR) singular field [9, 10] may not be valid in the case of a certain amount of crack extension where J ceases to act as amplifier for this singular field. Nevertheless, possible error is considered tolerable if the relative amount of crack extension stays within a certain limit, and if elastic unloading and non-proportional plastic loading zones around a crack tip are surrounded by a much larger zone of nearly proportional loading controlled by the HRR field. Under this condition of J-dominance, both the onset and limited amount of crack growth can be correlated to the critical values of J and J-resistance curve, respectively [11].

Consider Fig. 1 which illustrates a typical pipe with mean radius R, wall thickness t and a circumferential through-wall crack of total angle 2θ and length $2a = 2R\theta$. Suppose that the TWC pipe, which has length L, is subject to pure bending moment M (Fig. 1). It is assumed that the value of L is large enough so that there are no effects of boundary conditions on the crack driving force. The constitutive law characterizing the material's stress–strain response is represented by the well-known Ramberg Osgood model

$$\frac{\epsilon}{\epsilon_0} = \frac{\sigma}{\sigma_0} + \alpha\left(\frac{\sigma}{\sigma_0}\right)^n, \tag{1}$$

in which σ_0 is a reference stress which can be arbitrary, but is usually assumed to be the yield stress, E is the modulus of elasticity, $\epsilon_0 = \sigma_0/E$ is the associated reference strain, and α and n are model parameters usually chosen from best fit of actual laboratory data. Also, the J-resistance curve from the compact tension specimen is deemed to be adequately characterized by a power-law equation

$$J_R(\Delta a) = J_{1c} + C\left(\frac{\Delta a}{k}\right)^m, \tag{2}$$

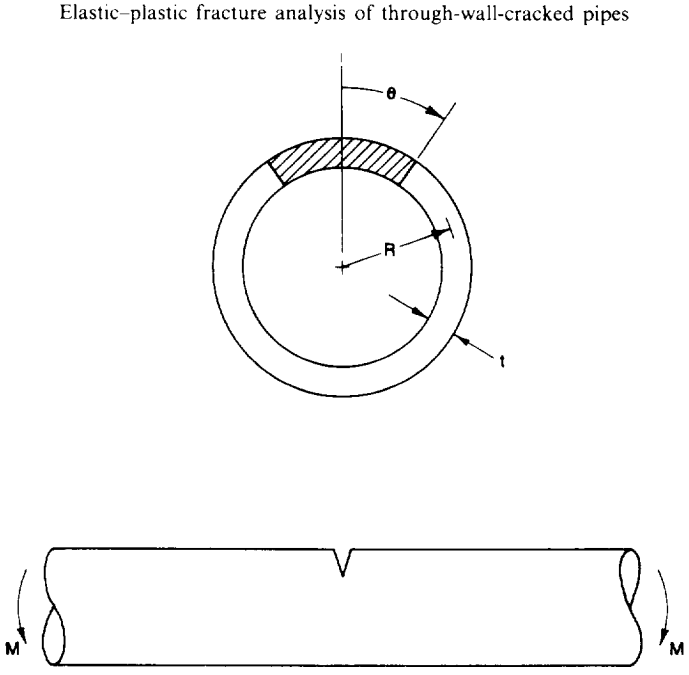

Fig. 1. A pipe with a circumferential through-wall crack subject to pure bending.

in which $\Delta a = R\,\Delta\theta$ is the crack length extension during crack growth, J_{Ic} is the fracture toughness at crack initiation, and C and m are model parameters also obtained from best fit of experimental data. The dummy parameter k, which has a value of 1, is introduced in eq. (2) only to dimensionalize C (e.g. when Δa is expressed in mm and $k = 1$ mm, then C has the same dimension as J). Note that "Δa" here is the physical crack extension, i.e. without blunting. This is because blunting is automatically accounted for in the pipe estimation schemes as well as finite element analysis.

2.1. *The J-integral*

Consider a cracked pipe with an arbitrary counter-clockwise path Γ around the crack tip. The J-integral is defined by [7–14]

$$J = \int_{\Gamma} \left(W\,\mathrm{d}y - T_i \frac{\partial u_i}{\partial x}\,\mathrm{d}s \right), \tag{3}$$

where x and y are co-ordinate axes with the crack tip as their origin, u_i and $T_i = \sigma_{ij} n_j$ are the ith components of displacements and traction vectors, n_j is the jth component of the unit outward normal to the integration path, $\mathrm{d}s$ is the differential length along contour Γ and $W = \int \sigma_{ij}\,\mathrm{d}\epsilon_{ij}$ is the strain energy density with σ_{ij} and ϵ_{ij} representing components of stress and strain tensors, respectively. For a pure power-law type constitutive equation, e.g. the Ramberg–Osgood model in eq. (1) [minus the elastic term] and mode-I loading, the stress and strain fields ahead of the crack tip are [7–14]

$$\sigma_{ij} = \sigma_0 \left[\frac{EJ}{\alpha \sigma_0^2 I_n r} \right]^{1/(n+1)} \tilde{\sigma}_{ij}(n, \theta) \tag{4}$$

$$\epsilon_{ij} = \frac{\alpha \sigma_0}{E} \left[\frac{EJ}{\alpha \sigma_0^2 I_n r} \right]^{n/(n+1)} \tilde{\epsilon}_{ij}(n, \theta), \tag{4}$$

where I_n is an integration constant that depends on n, $\tilde{\sigma}_{ij}(n, \theta)$ and $\tilde{\epsilon}_{ij}(n, \theta)$ are dimensionless functions, J is the path-independent integral defined by eq. (3), and r and θ are polar co-ordinates with the crack tip as their origin. The parameters I_n, $\tilde{\sigma}_{ij}(n, \theta)$ and $\tilde{\epsilon}_{ij}(n, \theta)$ also depend on the state of stress, i.e. on plane stress or plane strain condition. The above equations are the well-known HRR singularity field.

The J-integral defines the amplitude of the HRR singularity field, just as the stress intensity factor characterizes the amplitude of the stress field in linear-elastic fracture mechanics (LEFM). Thus, J completely describes the conditions within the plastic zones. A cracked structure in small-scale yielding has two singularity-dominated zones: one in the elastic region, where stress varies as $r^{-1/2}$ and one in the plastic zone, where stress varies as $r^{-1/(n+1)}$. In EPFM, the latter often persists long after the linear-elastic singularity zone has been destroyed by crack tip plasticity.

Under elastic–plastic condition, when the stress–strain curve is modeled by eq. (1), the total crack driving force J can be obtained by adding the elastic component J_e and plastic component J_p, i.e.

$$J = J_e + J_p. \tag{5}$$

For a TWC pipe under pure bending, closed-form expressions can be developed for both J_e and J_p. They are described below.

2.1.1. *Elastic solution for TWC pipe.* The elastic component J_e is given by [12–14]

$$J_e = \frac{K_I^2}{E}, \tag{6}$$

where K_I is the mode-I stress intensity factor in which plane stress condition is assumed. From LEFM theory, K_I can be obtained as

$$K_I = \frac{M}{\pi R^2 t} F\left(\frac{\theta}{\pi}, \frac{R}{t}\right)\sqrt{\pi R\theta}, \tag{7}$$

where $F(\theta/\pi, R/t)$ is a dimensionless function that depends on pipe and crack geometry. Hence, the elastic J is

$$J_e = \frac{\theta}{\pi} F\left(\frac{\theta}{\pi}, \frac{R}{t}\right)^2 \frac{M^2}{ER^3t^2}. \tag{8}$$

2.1.2. *Plastic solution for TWC pipe.* From eq. (4), the plastic component J_p in terms of applied stress is

$$J_p = \frac{\alpha\sigma_0^2}{E} I_n r\left[\frac{\sigma_{ij}}{\sigma_0}\right]^{n+1} \frac{1}{\tilde{\sigma}_{ij}^{n+1}}. \tag{9}$$

For J-controlled condition, the loading must be proportional, i.e. the local stresses must increase in proportion to the remote applied load, M. Therefore, for the pipe crack problem, eq. (9) can be written more specifically as [12–14]

$$J_p = \frac{\alpha\sigma_0^2}{E} R\theta\left(1 - \frac{\theta}{\pi}\right) h_1\left(\frac{\theta}{\pi}, n, \frac{R}{t}\right)\left[\frac{M}{M_0}\right]^{n+1}, \tag{10}$$

in which $h_1(\theta/\pi, n, R/t)$ is another dimensionless function that depends on pipe geometry, crack geometry and material constant, and

$$M_0 = 4\sigma_0 R^2 t\left[\cos\frac{\theta}{2} - \frac{1}{2}\sin\theta\right], \tag{11}$$

is a conveniently defined reference load that represents the limit-load for a TWC pipe under pure bending if σ_0 is the collapse stress. Thus, for a given TWC pipe if F and h_1 are known, the crack driving force J can be predicted readily.

2.2. *Evaluation of* F- *and* h_1*-functions*

2.2.1. *Finite element analysis.* The influence functions, $F(\theta/\pi, R/t)$ and $h_1(\theta/\pi, n, R/t)$, can be computed by using the finite element method (FEM). Computations of this kind for through-wall-cracked pipes were first reported by Kumar and coworkers [13, 14]. The finite element analyses by Kumar and coworkers [13, 14] involved computer code ADINA [15] using nine-noded shell

elements with three displacement and two rotational degrees of freedom at each node. The elements had only one node in the thickness direction. No special elements were needed to account for plastic incompressibility since the TWC pipe under tension or bending is essentially a plane stress problem [13, 14]. J was calculated by the virtual crack extension technique [13, 14]. In refs [13, 14], these influence functions are cataloged at several discrete values of parameters θ/π, n and R/t. For a given pipe with arbitrary values of these parameters, the corresponding F- and h_1-functions can be determined via interpolation or extrapolation of these tabulated values.

In a recent study at Battelle, these influence functions were examined to determine their adequacy for flaw evaluation of pipes with circumferential through-wall cracks. From preliminary evaluations, it was found that (1) the compiled values of h_1, and hence J_p, are too large especially when the hardening exponent n is large and/or the crack size θ/π is small, (2) for small crack sizes, the pipe rotations due to the crack are negative for both elastic and plastic solutions, and (3) no solutions are made available for $n = 10$ and some of $n = 7$ cases due to reported numerical difficulties. Some of these difficulties may be due to the use of simple nine-noded shell elements that could have produced overly stiff results [16, 17]. In consequence, the above influence functions were recomputed with particular attention to pipes with short through-wall cracks (e.g. when $\theta/\pi \leqslant 1/8$). In these new calculations several load cases, e.g. tension, bending, and combined bending and tension, were considered. Figure 2 shows a typical finite element mesh for a TWC pipe. Due to symmetry, only a quarter of the pipe was needed to be modeled. In all cases, 20-noded isoparametric brick elements were used with adequate refinement at the crack tip. Only one element through the pipe wall thickness was used and as such, the results should be viewed as average values through the pipe wall. The elastic solutions were developed using the elastic properties of pipe. A deformation theory of plasticity algorithm in the ABAQUS finite element code [18] was used to generate the plastic solution. A reduced 2×2 Gauss quadrature integration rule was utilized. J was calculated by the contour integral defined by eq. (3). The calculations were carried out for $\theta/\pi = 1/16$, $1/8$, $1/4$ and $1/2$, $n = 1, 2, 3, 5, 7$ and 10, and $R/t = 5, 10$ and 20. No numerical difficulties were encountered. Further details are available in Brust *et al.* [17, 19].

2.2.2. *Multivariate response surface approximations.* Following explicit finite element (ABAQUS) calculations of F- and h_1-functions at the pre-determined values of θ/π, n and R/t, multivariate response surface approximations are developed in this paper for $F(\theta/\pi, R/t)$ and $h_1(\theta/\pi, n, R/t)$. They are as follows:

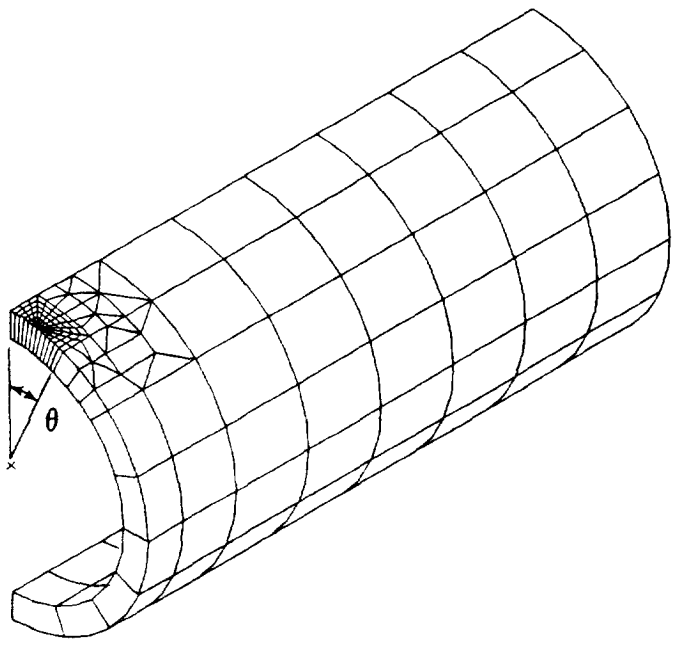

Fig. 2. Finite element idealization for a quarter pipe with a through-wall crack.

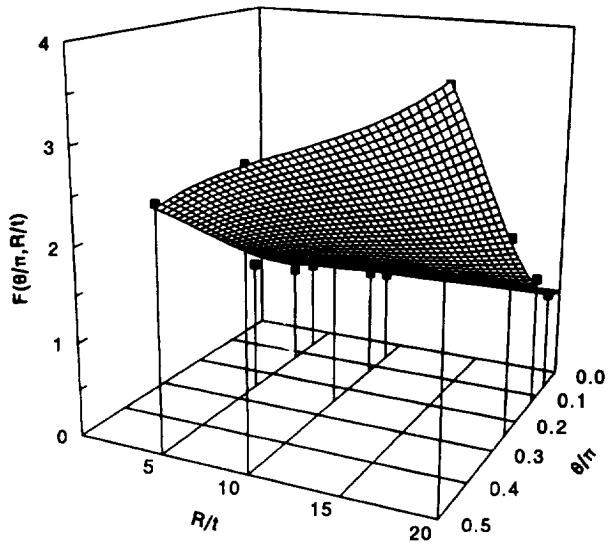

Fig. 3. Surface plot of proposed F-function.

F-*function*. The F-function can be approximated by

$$F\left(\frac{\theta}{\pi}, \frac{R}{t}\right) = 1 + \{A_1 \quad A_2 \quad A_3\} \begin{Bmatrix} \left(\frac{\theta}{\pi}\right)^{1.5} \\ \left(\frac{\theta}{\pi}\right)^{2.5} \\ \left(\frac{\theta}{\pi}\right)^{3.5} \end{Bmatrix} \{B_1 \quad B_2 \quad B_3 \quad B_4\} \begin{Bmatrix} 1 \\ \left(\frac{R}{t}\right) \\ \left(\frac{R}{t}\right)^2 \\ \left(\frac{R}{t}\right)^3 \end{Bmatrix}, \tag{12}$$

where the constant coefficients $A_i (i = 1\ 3)$ and $B_i (i = 1\ 4)$ are calculated from best fit of FEM results. The values of these coefficients are provided in Appendix A. Using these values, Fig. 3 shows a surface plot of F defined by eq. (12) as a function of θ/π and R/t. The points with the droplines in this figure represent the values from the ABAQUS finite element calculations [17–19].

h_1-*function*. The h_1-function can be approximated by

$$h_1\left(\frac{\theta}{\pi}, n, \frac{R}{t}\right) = \left\{1 \quad \left(\frac{\theta}{\pi}\right) \quad \left(\frac{\theta}{\pi}\right)^2 \quad \left(\frac{\theta}{\pi}\right)^3\right\} \begin{bmatrix} C_{00} & C_{10} & C_{20} & C_{30} \\ C_{01} & C_{11} & C_{21} & C_{31} \\ C_{02} & C_{12} & C_{22} & C_{32} \\ C_{03} & C_{13} & C_{23} & C_{33} \end{bmatrix} \begin{Bmatrix} 1 \\ n \\ n^2 \\ n^3 \end{Bmatrix}, \tag{13}$$

where the coefficients $C_{ij} (i, j = 0\text{–}3)$ depend only on the R/t ratio and are calculated as well. Appendix A also provides the values of C_{ij} for $R/t = 5$, 10 and 20. Using these values and eq. (13), Figs 4–6 show the surface plots of h_1 as functions of θ/π and n for $R/t = 5$, 10 and 20, respectively. As before, the points with the droplines in these figures represent the values from the ABAQUS finite element calculations [17–19].

2.2.3. *Comparisons with other solutions*. In order to evaluate eqs (12) and (13), other solutions of F- and h_1-functions, which are available in the literature, are compiled. They include analytical solutions by Sanders' energy release rate (elastic) formula [20, 21], analytical solutions by Klecker *et al.* [22] and Zahoor [23], and extensive finite-element calculations by Kumar and coworkers [13, 14], and Brust *et al.* [17, 19]. Figure 7 shows the comparisons of proposed F with these solutions as a function of crack size θ/π for $R/t = 5$, 10 and 20. As expected, eq. (12) agrees very well with all FEM calculations by Battelle. There is little difference between the FEM results by

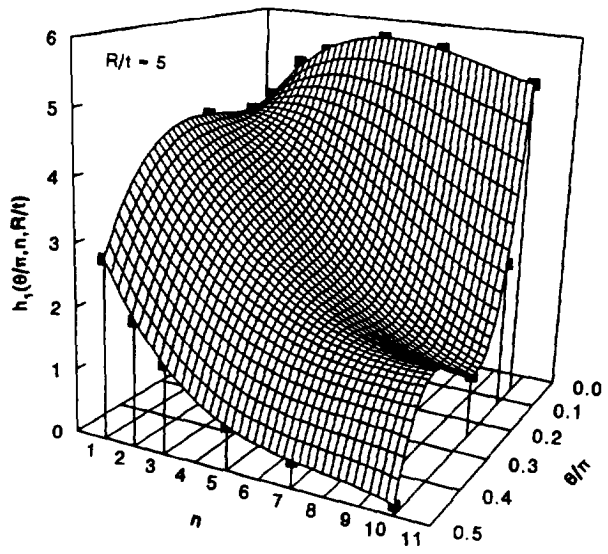

Fig. 4. Surface plot of proposed h_1-function for $R/t = 5$.

Battelle and GE/EPRI when the crack size is smaller (e.g. $\theta/\pi \leqslant 1/8$). However, for large crack size and large $R/t = 20$, the values of F produced by Battelle FEM are slightly greater than those generated by GE/EPRI FEM. The Sanders' solutions provide accurate results for large cracks, but can be overly unconservative for small cracks. In the limit when θ/π approaches zero, the Sanders' solutions do not converge to unity. The solutions by Klecker *et al.*, which were developed based on Sanders' solutions with corrections for small cracks, are closer to the GE/EPRI solutions. The solutions by Zahoor appear to fall inbetween the FEM results of Battelle and GE/EPRI.

Figure 8 shows similar plots of h_1 as a function of material constant n for several cases of crack size $\theta/\pi = 1/16, 1/8, 1/4$ and $1/2$, and $R/t = 5, 10$ and 20 by various methods. As before, the solutions include finite element calculations by Battelle [17, 19] and GE/EPRI [13, 14]. However, no analytical solutions are available for calculating h_1 due to the complexity of the problem. From Fig. 8, there are some differences between the FEM results of GE/EPRI and Battelle when the crack size is small (e.g. $\theta/\pi \leqslant 1/8$) and/or the material hardening exponent n is large (e.g. $n \geqslant 5$). In those cases, the values of h_1 produced by GE/EPRI FEM are always greater than those generated by Battelle. Hence, for short TWC cracked pipes with ferritic steel or ferritic/austenitic welds (which are usually associated with large n), the prediction of load-carrying capacity based on GE/EPRI

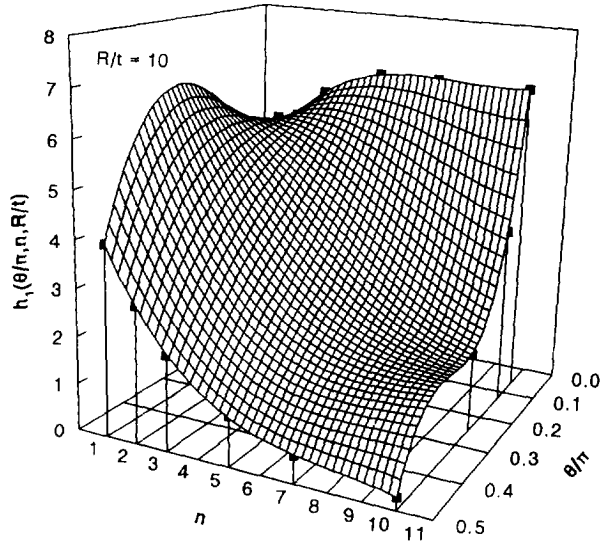

Fig. 5. Surface plot of proposed h_1-function for $R/t = 10$.

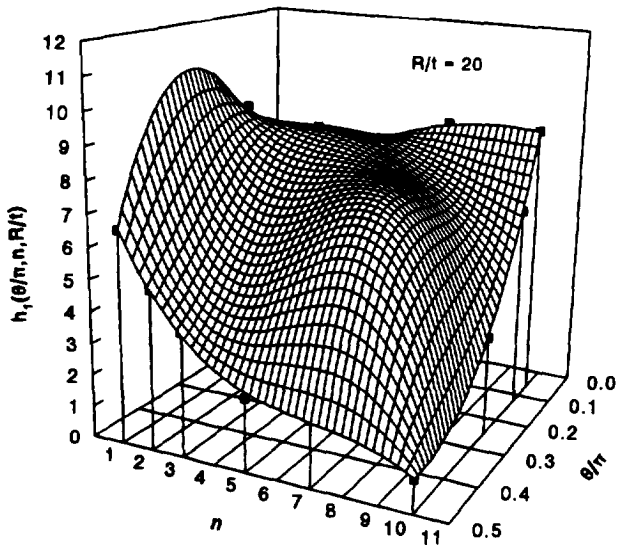

Fig. 6. Surface plot of proposed h_1-function for $R/t = 20$.

influence functions can be somewhat conservative. This is consistent with the author's past experience during analysis of full-scale pipe fracture experiments routinely conducted at Battelle [19, 24–26]. Also, for large R/t (e.g. $R/t = 20$), some differences may also exist between these FEM solutions. Further details on the comparisons of results for other influence functions for crack opening displacement, pipe displacement and pipe rotation are discussed in refs [17, 19].

The F- and h_1-functions developed in this paper [eqs (12) and (13)] should be applicable for $1/16 \leqslant \theta/\pi \leqslant 1/2$, $1 \leqslant n \leqslant 10$ and $5 \leqslant R/t \leqslant 20$. For the values of parameters outside these ranges, they are not verified here due to the scarcity of corresponding FEM results.

3. FAILURE LOAD

In order to evaluate structural integrity, it is required to know the load-carrying capacity of a piping system. There are several means by which it can be estimated. They are based on various definitions of failure criteria, e.g. initiation of crack growth and unstable crack growth in elastic–plastic fracture mechanics, and the Net-Section-Collapse in limit-load analysis. They are briefly described below.

3.1. *Initiation load*

The initiation load M_i can be defined as the bending moment which corresponds to initiation of crack growth in a pipe. If J is a relevant crack driving force, it can be estimated by solving the following nonlinear equation

$$f(M_i) \overset{\text{def}}{=} J(M_i, a) - J_{Ic} = 0, \tag{14}$$

in which $J(M_i, a)$ is the energy release rate (i.e. J-integral) for load M_i and crack size $a = R\theta$, which can be obtained from eqs (5), (8) and (10), and J_{Ic} is the fracture toughness at crack initiation. J_{Ic} can be determined from a standard compact tension test at the laboratory [3, 24]. Standard numerical methods, e.g. the bisection method, Newton–Raphson method and others, can be applied to solve eq. (14) [27].

3.2. *Maximum load*

In applications of nonlinear fracture mechanics, particularly for nuclear power plants, the J-tearing theory is a very prominent concept for calculating the maximum load-carrying capacity of a pipe. It is based on the fact that fracture instability can occur after some amount of stable crack growth in tough and ductile materials, with an attendant higher applied load level at fracture. Let J and J_R denote the crack driving force and toughness of a ductile piping material as a function

of load and crack size. The limit state characterizing fracture instability based on J-tearing theory is given by

$$f_1(M_{\max}, a^*) \overset{\text{def}}{=} J(M_{\max}, a^*) - J_R(a^* - a) = 0 \tag{15}$$

and

$$f_2(M_{\max}, a^*) \overset{\text{def}}{=} \frac{\partial J}{\partial a}(M_{\max}, a^*) - \frac{\mathrm{d}J_R}{\mathrm{d}a}(a^* - a) = 0, \tag{16}$$

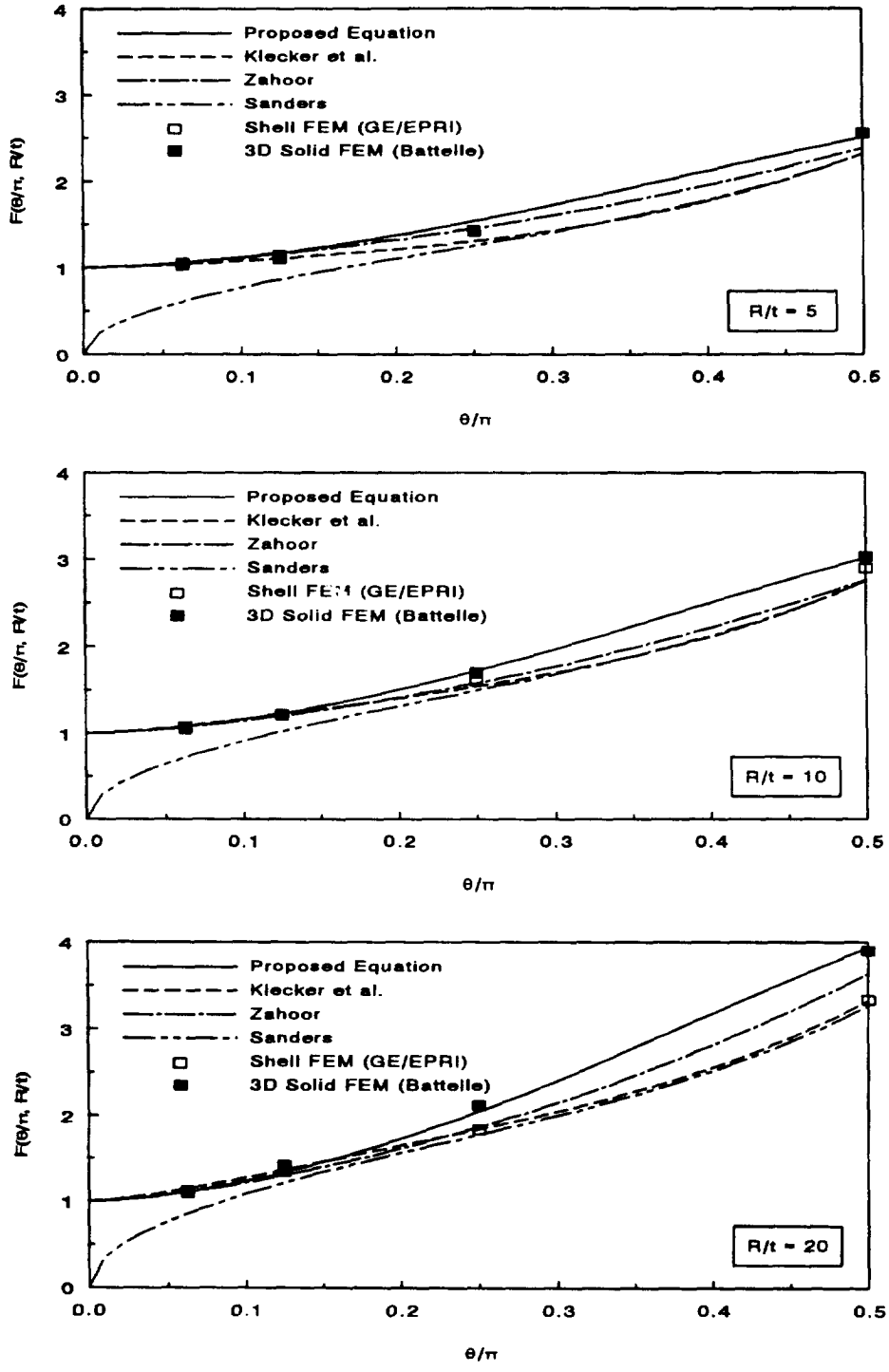

Fig. 7. Comparisons of F-functions by various methods.

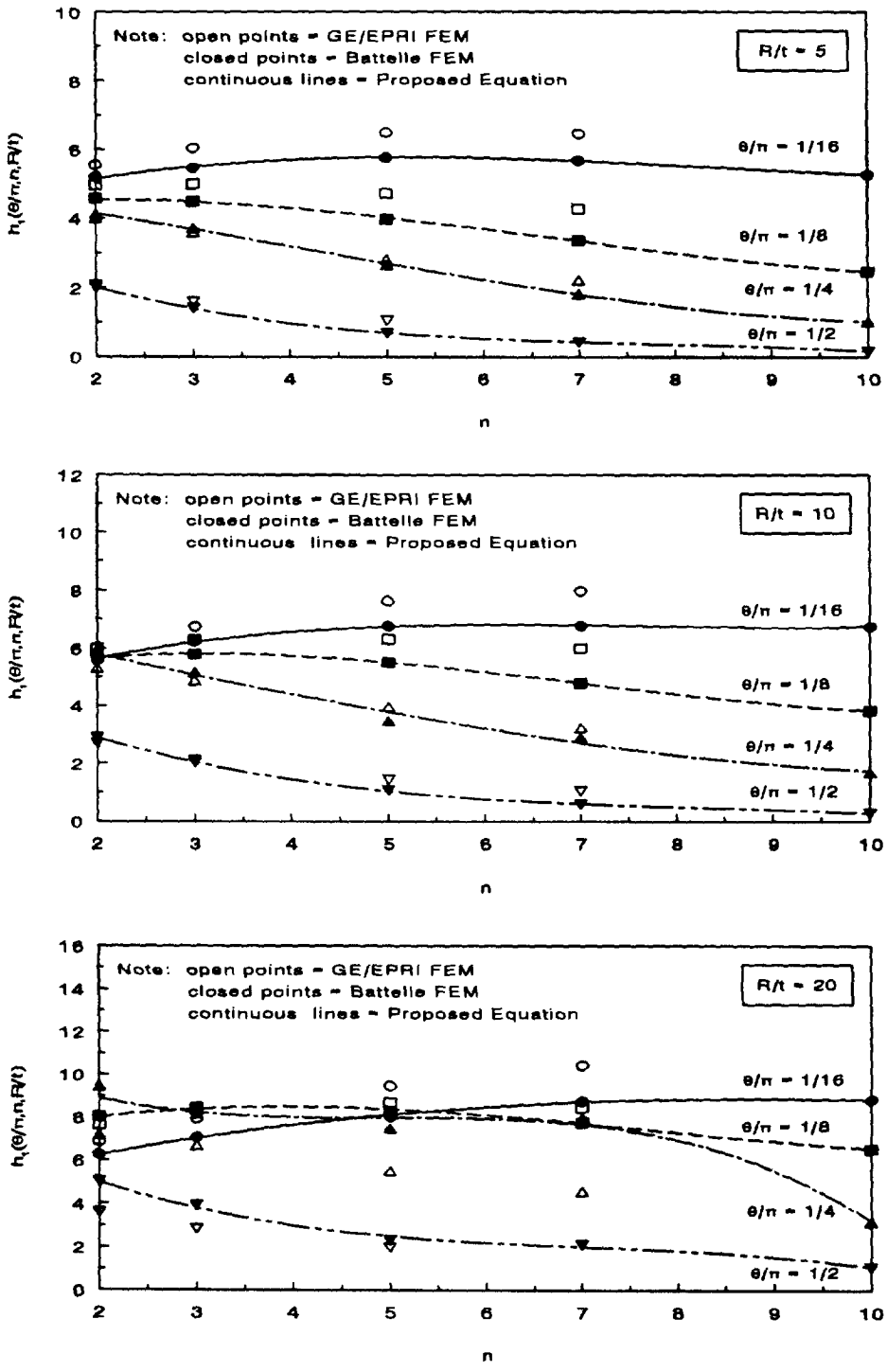

Fig. 8. Comparisons of h_1-functions by various methods.

where M_{max} and a^* represent load and half the crack length when crack growth becomes unstable. Equations (15) and (16) are two nonlinear simultaneous equations with the independent variables M_{max} and a^*. Once again, they can be solved by standard methods, e.g. the Newton–Raphson method [27].

3.3. *Net-Section-Collapse load*

The Net-Section-Collapse analysis is a simple, straightforward failure prediction method for TWC pipes in pure bending. In this analysis, it is assumed that (1) the failure load occurs when

the pipe section containing the crack becomes fully plastic, (2) there is insignificant crack growth from crack initiation to failure and (3) the toughness of the material is sufficiently high so that failure is governed by the strength of materials (i.e. the flow or collapse stress). The collapse stress is a value between the yield and ultimate strengths of a material and represents an average critical net-section stress throughout the uncracked ligament of the structure. Based on these assumptions, the Net-Section-Collapse load M_{nsc} is given by [28]

$$M_{nsc} = 4\sigma_f R^2 t\left(\cos\frac{\theta}{2} - \frac{1}{2}\sin\theta\right). \tag{17}$$

where σ_f is the flow or collapse stress. In this paper, σ_f is assumed to be the average of yield and ultimate strengths of the pipe material.

4. RANDOM PARAMETERS AND SYSTEM RESPONSE

Consider a cracked pipe with uncertain mechanical and geometric characteristics that is subject to random loads. Denote by $\mathbf{X}$ an n-dimensional random vector with components $X_1, X_2, \ldots, X_N$ characterizing uncertainty in the system and load parameters. For example, when a TWC pipe is considered, the possible random components are: crack size θ/π, pipe radius-to-thickness (R/t) ratio, elastic modulus E, basic strength parameters σ_y and σ_u, Ramberg–Osgood constitutive parameters α and n, fracture toughness parameters J_{Ic}, C and m, applied bending moment M. All or some of these variables can be modeled as random variables. Hence, any relevant response, such as the J-integral, should be evaluated by the probability

$$F_J(j_0) \overset{\text{def}}{=} \Pr[J(\mathbf{X}) < j_0] \overset{\text{def}}{=} \int_{J(\mathbf{x}) < j_0} f_{\mathbf{X}}(\mathbf{x})\,d\mathbf{x}, \tag{18}$$

where $F_J(j_0)$ is the cumulative probability distribution function of J and $f_{\mathbf{X}}(\mathbf{x})$ is the known joint probability density function of random vector $\mathbf{X}$.

The above fracture parameter J can also be applied to determine the load-carrying capacity of TWC pipes. Several fracture criteria based on this J-integral parameter and Net-Section-Collapse are discussed in Section 3. In a generic sense, let $M_f(\mathbf{X})$ denote the failure moment for a given TWC pipe under pure bending. Note that $M_f(\mathbf{X})$ is always random because it depends on input vector $\mathbf{X}$ which is random. It can be evaluated when a relevant crack driving force from deterministic fracture [e.g. J-integral from finite element analysis or eqs (8) and (10)] and an appropriate fracture criterion [e.g. eq. (14) or eqs (15) and (16)] are known. Suppose that the design requires $M_f(\mathbf{X})$ to always be greater than the applied load M (M can be random as well). This requirement cannot be satisfied with certainty because both the system and load parameters are uncertain. Hence, the performance of the pipe should be evaluated by the reliability P_S or its complement, the probability of failure, P_F ($P_S = 1 - P_F$) defined as

$$P_F \overset{\text{def}}{=} \Pr[g(\mathbf{X}) < 0] \overset{\text{def}}{=} \int_{g(\mathbf{x}) < 0} f_{\mathbf{X}}(\mathbf{x})\,d\mathbf{x}, \tag{19}$$

where the $g(\mathbf{X})$ is the performance function given by

$$g(\mathbf{X}) - M_f - M = S(\sigma_y, \sigma_u, \alpha, n, J_{Ic}, C, m, \theta/\pi, R/t, E) - M, \tag{20}$$

in which S is a function (implicit) of random parameters characterizing the pipe's structural resistance [only the random arguments are shown in eq. (20)]. A wide variety of failure probability, defined by eq. (19), can be evaluated if the appropriate fracture criterion is known. For example, when $M_f(\mathbf{X})$ is equal to the initiation load $M_i(\mathbf{X})$, P_F in eq. (19) corresponds to the probability of initiation of crack growth which provides a conservative estimate of the pipe's structural performance. A more realistic evaluation of the pipe's reliability can be evaluated if $M_f(\mathbf{X})$ is equal to the maximum load $M_{max}(\mathbf{X})$ (which allows the crack to grow until it becomes unstable) in which case P_F represents failure probability due to the exceedance of the pipe's maximum load-carrying capacity. When EPFM-based failure criteria are not necessary, the simple performance function based on limit-load analysis [i.e. $M_f(\mathbf{X}) = M_{nsc}(\mathbf{X})$] can also be used to determine failure probability of pipes.

5. STRUCTURAL RELIABILITY ANALYSIS

The generic expressions for both probabilities in eqs (18) and (19) involve multi-dimensional probability integration for their evaluation. In this regard, standard reliability methods such as First- and Second-Order Reliability Methods (FORM/SORM) [29–35] and simulation methods, e.g. Importance Sampling (IS) [35–40], Directional Simulation [41–44], Monte Carlo Simulation (MCS) [35, 45] and others, can be applied to compute these probabilities. In this paper, FORM/SORM, Importance Sampling and MCS methods are used for structural reliability analysis. They are briefly described here to compute the probability of failure P_F in eq. (19) assuming a generic N-dimensional random vector $\mathbf{X}$ and the performance function $g(\mathbf{x})$ defined by eq. (20). The same methods can be applied to determine the probability $F_J(j_0)$ defined by eq. (18).

5.1. *First- and Second-Order Reliability Methods (FORM/SORM)*

First- and Second-Order Reliability Methods are general methods of structural reliability theory. The methods are based on linear (first-order) and quadratic (second-order) approximations of the limit state surface $g(\mathbf{x}) = 0$ tangent to the closest point of the surface to the origin of the space. The determination of this point involves nonlinear programming and is performed in the standard Gaussian image of the original space. The FORM/SORM algorithms involve several steps. First, the space of uncertain parameters $\mathbf{x}$ is transformed into a new N-dimensional space $\mathbf{u}$ consisting of independent standard Gaussian variables. The original limit state $g(\mathbf{x}) = 0$ then becomes mapped onto the new limit state $g_U(\mathbf{u}) = 0$ in the $\mathbf{u}$ space. Second, the point on the limit state $g_U(\mathbf{u}) = 0$ having the shortest distance to the origin of the $\mathbf{u}$ space is determined by using an appropriate nonlinear optimization algorithm. This point is referred to as the design or β-point, and has a distance β_{HL} to the origin of the $\mathbf{u}$ space. Third, the limit state $g_U(\mathbf{u}) = 0$ is approximated by a surface tangent to it at the design point. Let such limit states be $g_L(\mathbf{u}) = 0$ and $g_Q(\mathbf{u}) = 0$, which correspond to approximating surfaces of hyperplane (linear or first-order) and hyperparaboloid (quadratic or second-order), respectively. The probability of failure P_F [eq. (19)] is thus approximated by $\Pr[g_L(\mathbf{u}) < 0]$ in FORM and $\Pr[g_Q(\mathbf{u}) < 0]$ in SORM. These first- and second-order estimates $P_{F,1}$ and $P_{F,2}$ are given by [29–35]

$$P_{F,1} = \Phi(-\beta_{HL})$$
$$P_{F,2} \simeq \Phi(-\beta_{HL}) \prod_{i=1}^{N-1} (1 - \kappa_i \beta_{HL})^{-1/2}, \tag{21}$$

where

$$\Phi(u) = \frac{1}{\sqrt{2\pi}} \int_{-\infty}^{u} \exp(-\tfrac{1}{2}\xi^2)\, d\xi \tag{22}$$

is the cumulative distribution function of a standard Gaussian random variable, and κ_i's are the principal curvatures of the limit state surface at the design point. FORM/SORM are analytical probability computation methods. Each input random variable and the performance function $g(\mathbf{x})$ must be continuous. Depending on the solver for nonlinear programming, additional requirement regarding smoothness, i.e. differentiability of $g(\mathbf{x})$, may be required. Further details of FORM/SORM equations are given in Appendix B.

5.2. *Monte Carlo Simulation (MCS)*

Consider a generic N-dimensional random vector $\mathbf{X}$ which characterizes uncertainty in all load and system parameters with the known joint distribution function $F_{\mathbf{X}}(\mathbf{x})$. Suppose that $\mathbf{x}^{(1)}, \mathbf{x}^{(2)}, \ldots, \mathbf{x}^{(L)}$ are L realizations of input random vector $\mathbf{X}$ which can be generated independently. Appendix C provides a simple method to generate $\mathbf{X}$ from its known probability distribution. Let $g^{(1)}, g^{(2)}, \ldots, g^{(L)}$ be the output samples of $g(\mathbf{X})$ corresponding to the input $\mathbf{x}^{(1)}, \mathbf{x}^{(2)}, \ldots, \mathbf{x}^{(L)}$ that can be obtained by conducting repeated deterministic evaluation of the performance function in eq. (20). Define L_f as the number of trials which is associated with negative values of the performance function. Then, the estimate $P_{F,MCS}$ by simulation becomes

$$P_{F,MCS} = \frac{L_f}{L}, \tag{23}$$

which approaches the exact failure probability P_F when L approaches infinity. When L is finite, a statistical estimate on the probability estimator may be needed. In general, the required sample size must be at least 10/minimum (P_F, P_S) for a 30% coefficient of variation of the estimator [45].

5.3. *Importance Sampling*

In Importance Sampling, the random variables are sampled from a different probability density, known as the sampling density. The purpose is to generate more outcomes from the region of interest, e.g. the failure set $F = \{\mathbf{x}: g(\mathbf{x}) < 0\}$. Using information from FORM/SORM analyses, good sampling densities can be constructed. According to Hohenbichler [40], the failure probability estimate $P_{F,IS}$ by importance sampling based on SORM improvement is given by

$$P_{F,IS} \simeq \Phi(-\beta_{HL}) \prod_{i=1}^{N-1} [1 - \kappa_i \Psi(-\beta_{HL})]^{-1/2} \frac{1}{N_{IS}} \sum_{j=1}^{N_{IS}} \frac{\Phi[h_Q(\mathbf{w}_j)]}{\Phi(\beta_{HL})} \exp\left[-\tfrac{1}{2}\Psi(\beta_{HL}) \sum_{k=1}^{N-1} \kappa_k w_{k,j}^2\right], \tag{24}$$

where $\Psi(-\beta_{HL}) = \phi(-\beta_{HL})/\Phi(-\beta_{HL})$, $\mathbf{w}_j = \{w_{1,j}, w_{2,j}, \ldots, w_{N-1,j}\}^T$ is the jth realization of the independent Gaussian random vector $\mathbf{W}$ with the mean and variance of ith component being zero and $1/[1 - \Psi(-\beta_{HL})]$, $h_Q(\mathbf{w}_j)$ is the quadratic approximant in the form of rotational hyper-paraboloid and N_{IS} is the sample size for importance sampling. Further details are given in Appendix B and are also available elsewhere [35, 40].

6. NUMERICAL APPLICATIONS

6.1. *Description of the problem*

Consider a TWC side riser pipe made of Type 304 stainless steel from a Boiling Water Reactor plant with outer diameter $D_0 = 709.17$ mm (27.92 in.), pipe wall thickness $t = 33.77$ mm (1.33 in.) and elastic modulus $E = 182.700$ MPa (26.500 ksi). They are assumed to be deterministic. The random parameters include crack size θ/π, yield strength σ_y, ultimate strength σ_u, Ramberg–Osgood constitutive parameters α and n, and fracture toughness parameters J_{Ic}, C and m. The statistical properties of these variables are described below.

6.1.1. *Statistical characterization of material properties.* Samples of raw data for stress–strain and J-resistance curves of a specific pipe material (e.g. Type 304 stainless steel) are obtained from refs [1–6]. Each of these are then fitted with eqs (1) and (2) to determine the constitutive model parameters α and n, and fracture toughness parameters, J_{Ic}, C and m. During the calculation of Ramberg–Osgood parameters α and n, the reference stress σ_0 is assumed to be 152 MPa (22.05 ksi). The basic strength parameters, e.g. yield strength σ_y (0.2% offset) and ultimate strength σ_u, are determined as well. These provided the independent measurements of the random vectors $\{\sigma_y, \sigma_u\}^T$, $\{\alpha, n\}^T$ and $\{J_{Ic}, C, m\}^T$ representing pipe material properties. Standard statistical analyses are then conducted to determine their probabilistic characteristics. Table 1 shows the mean and covariance

Table 1. Mean and covariance of material properties for Type 304 stainless steel pipe

Random vector	Mean vector	Covariance matrix
$\begin{Bmatrix}\sigma_y\\ \sigma_u\end{Bmatrix}^{(a)}$	$\begin{Bmatrix}151.526\\ 450.632\end{Bmatrix}$	$\begin{bmatrix}220.881 & 118.615\\ 118.615 & 652.654\end{bmatrix}$
$\begin{Bmatrix}\alpha\\ n\end{Bmatrix}^{(b)}$	$\begin{Bmatrix}8.942\\ 3.615\end{Bmatrix}$	$\begin{bmatrix}10.920 & -1.202\\ -1.202 & 0.208\end{bmatrix}$
$\begin{Bmatrix}J_{Ic}\\ C\\ m\end{Bmatrix}^{(c)}$	$\begin{Bmatrix}1059.56\\ 345.087\\ 0.652\end{Bmatrix}$	$\begin{bmatrix}2.024 \times 10^5 & -58.937 & -25.530\\ -58.937 & 1.006 \times 10^4 & 6.842\\ -25.530 & 6.842 & 0.0242\end{bmatrix}$

(a) Both σ_y and σ_u are in MPa unit.
(b) α and n are dimensionless; $\sigma_0 = 152$ MPa; $E = 182{,}700$ MPa [eq. (1)].
(c) Both J_{Ic} and C are in kJ/m^2 unit with $k = 1$ mm [eq. (2)]; m is dimensionless; Δa is to be expressed in mm unit.

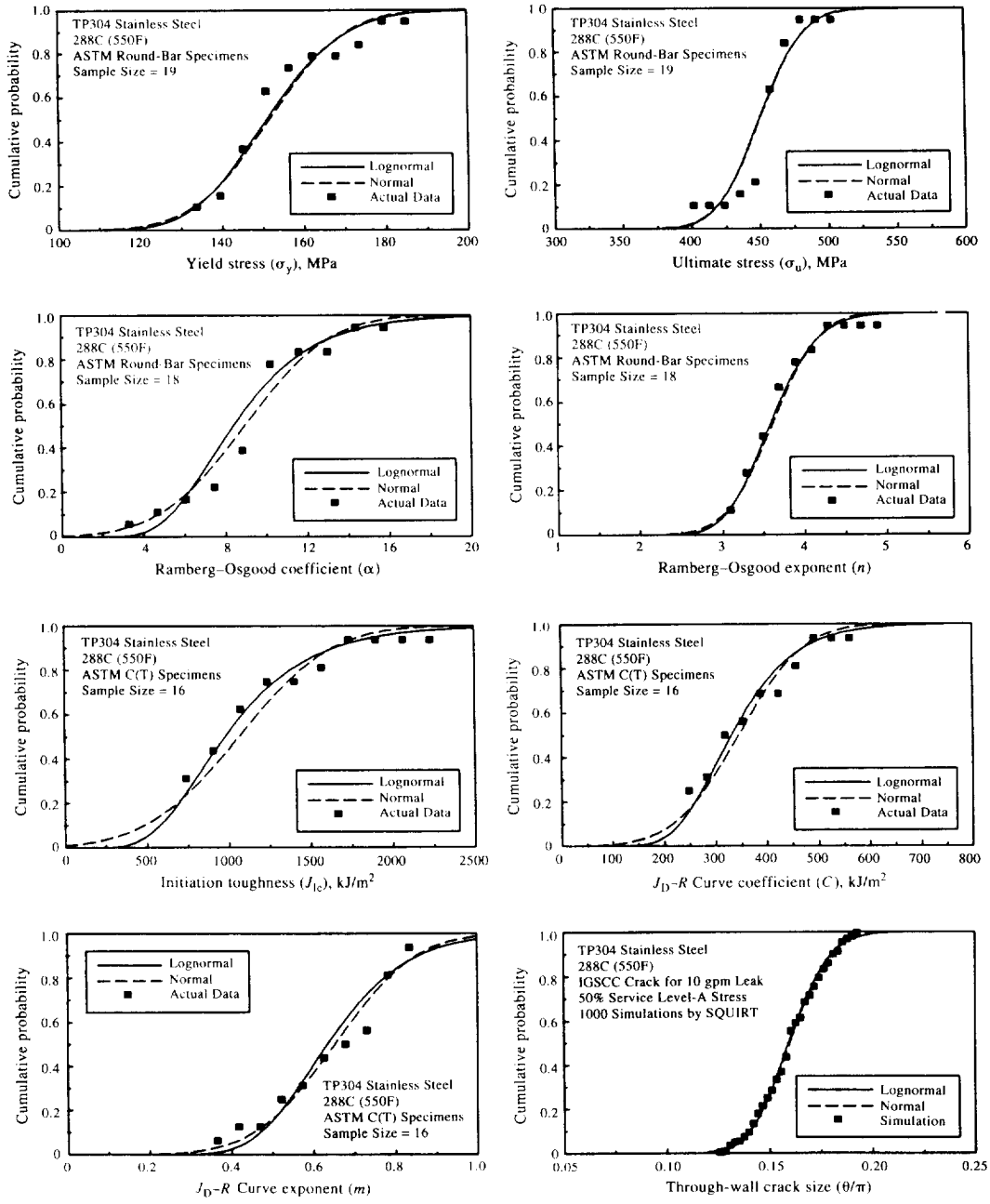

Fig. 9. Statistical characterization of random input variables.

for each of these random vectors. It is assumed that the joint probability distribution of each vector is lognormal. This is justified via comparisons with actual data in Fig. 9 which indicate that the marginal probability of each component of the above vectors follows the lognormal distribution reasonably well. A Gaussian distribution also seems to be a good choice, but there are some concerns over the possible negative realizations of some of these positive random variables which have large coefficients of variation. Hence, **X** will be modeled with lognormal probability although no rigorous proof is provided here to validate this assumption by comparing the multivariate joint probability distributions. Also, no correlations are permitted between the strength and toughness properties, because each set of laboratory data does not always include simultaneous measurement of all properties. However, the components within each vector are correlated and their correlation characteristics are defined in the covariance matrices provided in Table 1.

Methods to generate samples of random vector **X**, which are needed in FORM/SORM and simulation analyses, are described in Appendix C. For special cases, when **X** is either correlated normal or correlated lognormal, sample generation of **X** becomes much simpler. They are also explained in Appendix C.

6.1.2. *Statistical characterization of through-wall-crack size.* In order to perform probabilistic analysis, the probability distribution of initial crack size θ/π also needs to be specified. In this example problem, it is assumed that the TWC crack is located in the base metal of the pipe with the anticipated cracking mechanism being intergranular stress corrosion cracking (IGSCC). During a recent study by the author on probabilistic leak-before-break analysis (LBB) [46, 47], it was found that the leakage size flaw can be modeled by the lognormal or truncated normal distributions [48, 49]. The distribution parameters of this flaw size vary according to the leak-rate detection capability and applied normal stresses in the pipe. The analyses accounted for statistical variability of several crack morphology variables (e.g. surface roughness, number of turns or bends, path deviation factors, etc.) of IGSCC crack, which can affect the leak rate through cracks typically found in nuclear piping. Detailed results of these analyses are available in refs [48, 49]. Assuming that the initial crack is the LBB detectable flaw (leakage size crack), it is modeled here with lognormal probability distribution. When the normal operating stress is 50% of ASME Service Level-A stress (Service Level-A stress limit is equal to $1.5S_m$, where S_m is code-specified design stress defined in the ASME Section III, Appendix I [50]) and the leakage detection capability is 10 gpm, the mean value of θ/π is 0.16 with the coefficient of variation 9.69% for the side riser pipe considered in this example [48, 49]. Comparisons of lognormal (and also Gaussian) distribution with simulated (computed) distribution of θ/π are also shown in Fig. 9. Further details can be obtained from refs [48, 49].

6.2. *Probabilistic characteristics of J-integral*

The Second Order Reliability Method is applied to determine the probabilistic characteristics of the J-integral for the side riser pipe as a function of applied load. Figures 10 and 11 show the computed probability densities for several values of applied load $M = 1.0$ MNm, 1.5 MNm, 2.0 MNm and 3.0 MNm. They are obtained by repeated FORM/SORM analysis for various thresholds of J, i.e. by calculating the probability in eq. (18) as a function of j_0 and then taking the numerical derivative of this probability with respect to j_0. As expected, the probability mass shifts to the right when the applied loads are higher. Also presented in the same figures are the corresponding histograms of the J-integral developed by conducting direct Monte Carlo simulations for the same values of applied loads. The sample size for each Monte Carlo analysis is 10000. Comparisons with the SORM results indicate that this approximate method can

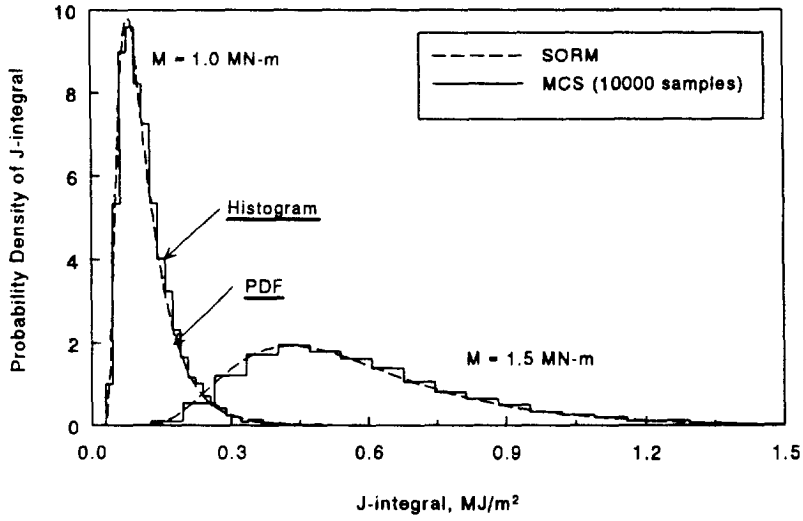

Fig. 10. Probabilistic characteristics of J-integral ($M = 0.5$ and 1 MNm).

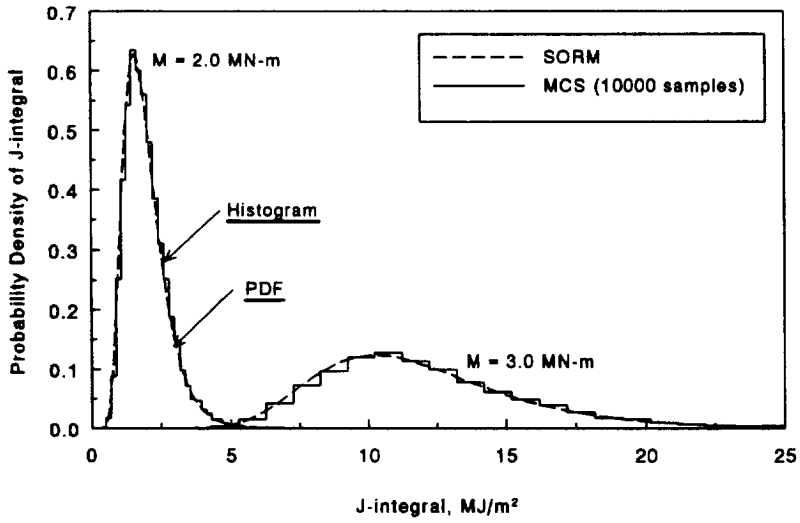

Fig. 11. Probabilistic characteristics of J-integral ($M = 2$ and 3 MNm).

predict probabilistic characteristics of J with very good accuracy for all values of applied load considered here.

6.3. *Reliability assessment of TWC pipes*

Figure 12 shows the plots of failure probability P_F vs applied moment M for the side riser pipe obtained for several definitions of failure load defined earlier. Various reliability methods, e.g. FORM and SORM, and simulation methods, e.g. Importance Sampling (IS) and MCS, are used to determine the failure probability. They all consistently indicate that P_F increases as M increases, and it approaches unity when M becomes very large. Based on the formulation of failure condition [eq. (19)], these curves also represent the cumulative probability distribution functions of the failure loads of the pipes. Compared with the failure probabilities due to pipe instability, the above results based on initiation of crack growth and Net-Section-Collapse are higher and lower, respectively. The results of Fig. 12 also address the applicability of Net-Section-Collapse equations which are widely used by engineers for pipe flaw evaluation in nuclear power plants. Unless there is sufficient evidence that the pipe will, indeed, fail with the limit-load criterion, an analysis based on the Net-Section-Collapse load (without any safety margin) may overpredict the reliability of pipes.

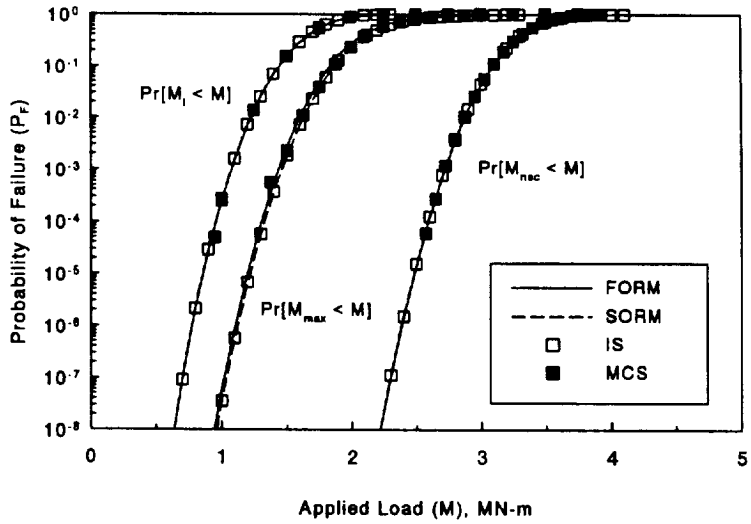

Fig. 12. Probability of failure by various methods.

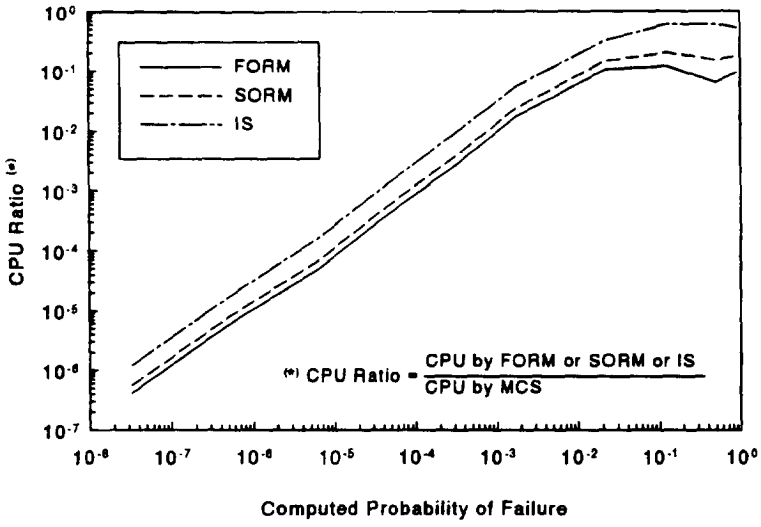

Fig. 13. Computational efficiency of FORM/SORM and Importance Sampling.

Figure 12 also shows that the results obtained from the approximate methods, e.g. FORM and SORM, provide satisfactory probability estimates when compared with "exact" results from Importance Sampling and MCS. No meaningful differences are found between the results of FORM and SORM, and their probability estimates are virtually identical. During the performance of MCS, the sample size is varied according to the level of probability being estimated. In all cases, the sample size has been targeted to be $10/\min(P_F, P_S)$ [with a minimum of 500] for obtaining a 30% coefficient of variation of the probability estimator.

Figure 13 exhibits the relative effort and computational expenses required to determine above solutions by FORM, SORM, IS and MCS methods. They are measured in terms of Central Processing Units (CPU) by executing computer codes for each of these methods. The plots in this figure show how the normalized ratio of CPU time required by FORM, SORM and IS (CPU ratio is defined as the ratio of CPU by each of these methods and the CPU by MCS) vary with the range of probability estimates made in this study. It appears that for values of failure probability approaching one, the CPU ratio also approaches one implying that the computational effort by each of the above four methods is very similar. However, when the failure probabilities are smaller, a significant amount of CPU time can be saved by using FORM, SORM and IS methods, instead of using MCS. A computational reduction in the order of 10^{-6} times the CPU required by MCS

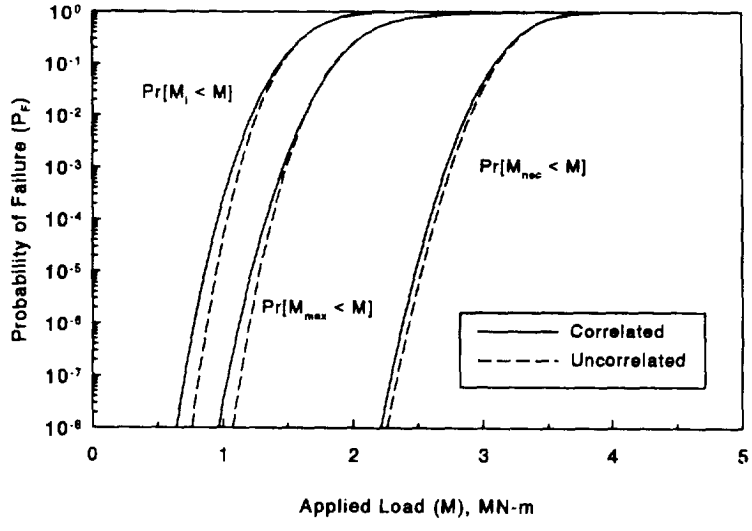

Fig. 14. Effects of correlation on failure probabilities of TWC pipes.

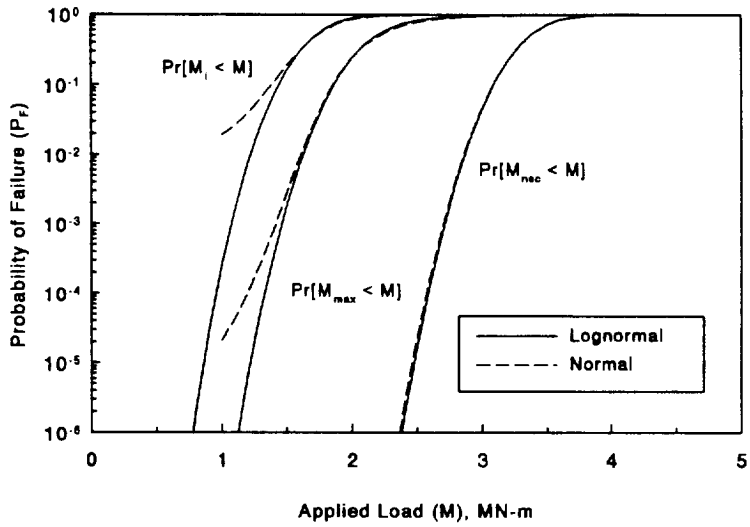

Fig. 15. Effects of input distributions on failure probabilities of TWC pipes.

has been observed in performing these pipe specific probability calculations. Also, the differences in CPU times consumed by FORM, SORM and IS analyses are quite negligible when compared with the magnitudes of CPU time required by MCS. Clearly, the FORM/SORM algorithms and Importance Sampling method are more efficient than direct MCS and become far superior particularly when the failure probabilities are in the lower range.

6.4. *Effects of correlation and probability distribution of input*

Figure 14 shows the plots of failure probability as a function of applied load when the correlation coefficient between any two input random variables is neglected. The probability distribution of **X** is, however, still lognormal with the same means and variances prescribed in Table 1. Comparisons of results suggest that the failure probability based on zero correlation is unconservative when compared with those based on actual correlations. Particularly, when the load is small, large differences in the failure probability associated with EPFM-based fracture criteria may exist and hence, correlation coefficients should not be neglected in those cases.

Figure 15 presents similar results to study the effects of probability distributions of input random variables on the failure probability. Both Gaussian and lognormal probabilities are assumed for joint distributions of random material properties and initial crack size. In both cases, the same mean vector and covariance matrices are assumed, and are defined in Table 1. From Fig. 15, it appears that probability distributions of input random variables with identical first- and second-moment characteristics can provide different values of failure probability when the performance criteria are based on the initiation and maximum loads. Differences in the results diverge rapidly when the applied load levels are smaller, for which cases probabilities are also smaller. Hence, careful attention should be given to determine the statistical characteristics of input as accurately as possible. All probabilities in Figs 14 and 15 are computed by SORM.

The above observations, however, appear to be irrelevant for pipe fracture evaluation based on Net-Section-Collapse load. This is mainly because for limit-load analysis (1) the number of random variables is fewer e.g. θ/π, σ_y and σ_u and (2) the variance (uncertainty) for each of these variables is smaller (see Table 1). Hence, both normal and lognormal distributions should provide fairly close failure probabilities.

7. SUMMARY AND CONCLUSIONS

A probabilistic model is developed for nonlinear fracture-mechanics analysis of through-walled-cracked pipes subject to bending loads. It involves elastic–plastic finite element analysis for estimating energy release rates, J-tearing theory for characterizing ductile fracture and standard structural reliability methods for conducting probabilistic analysis. Evaluation of the J-integral is

based on deformation theory of plasticity and power-law idealizations of stress–strain and fracture toughness curves. This allows the J-integral to be expressed in terms of non-dimensional influence functions (F- and h_1-functions) that depend on crack size, pipe geometry and material hardening constant. New equations are developed for these influence functions based on recent finite-element calculations at Battelle. The validity of proposed equations for predicting the crack driving force in TWC pipes is evaluated by comparing with available results in the literature.

A number of standard reliability methods is formulated to determine the probabilistic characteristics of the J-integral for a circumferential TWC pipe as a function of applied bending moment. The same methods are used later to compute failure probability of the cracked pipes. Several failure criteria associated with crack initiation, unstable crack growth and Net-Section-Collapse are used to determine such probabilities.

Numerical applications are provided to illustrate the proposed methodology. A nuclear piping made of Type 304 stainless steel (side riser pipe) from a Boiling Water Reactor plant is chosen to evaluate its probabilistic performance. First, the probability densities of the J-integral are predicted as a function of applied bending loads. Second, failure probabilities corresponding to various performance criteria are evaluated by standard structural reliability methods. Finally, sensitivity studies are performed to determine the effects of correlation and distribution properties of random input on the failure probability. Results suggest that

(1) current reliability methods, e.g. FORM and SORM, can provide accurate probabilistic characteristics of the J-integral and failure loads for TWC pipes under bending with much less computational effort when compared with those obtained from direct MCS. A computational reduction in the order of 10^{-6} times the CPU consumed by MCS has been observed in performing pipe specific probability calculations. Similar accuracy and computational efficiency by Importance Sampling method have also been demonstrated,

(2) failure probabilities due to the exceedance of initiation load and Net-Section-Collapse load are higher and lower, respectively, when compared with those due to the exceedance of maximum load of TWC pipes. Large differences may exist in the results produced by each of the three failure criteria, especially when the applied load levels are smaller, for which failure probabilities are also smaller. Unless there is adequate evidence that the pipe will fail with a limit-load criterion, an analysis based on Net-Section-Collapse load (without any safety margin) may overpredict the reliability of a piping system significantly and

(3) both correlation and probability distribution of input random variables can affect predictions of failure probability of TWC pipes based on EPFM-based performance criteria. These effects can become significant when the applied loads are smaller, for which cases failure probabilities are also smaller. However, when the failure load is based on limit-load analysis, they appear to have negligible effects due to fewer number and less uncertainty of the input random variables.

REFERENCES

[1] A. L. Hiser and G. M. Callahan, *A User's Guide to the NRC's Piping Fracture Mechanics Database (PIFRAC)*. NUREG/CR-4894, U.S. Nuclear Regulatory Commission, Washington, D.C., U.S.A. (1987).

[2] G. M. Wilkowski *et al.*, Degraded piping program—Phase II. Semiannual Reports from March 1984 to January 1985 NUREG/CR-4082, Vols 1–8, U.S. Nuclear Regulatory Commission, Washington, D.C., U.S.A. (1985–1989).

[3] R. A. Schmidt, G. M. Wilkowski and M. E. Mayfield, The international piping integrity research group (IPIRG) program—an overview. *Proc. 11th Int. Conf. Structural Mechanics in Reactor Technology, Vol. G2: Fracture Mechanics and Non-Destructive Evaluation*—2 (pp. 177–188), Tokyo, Japan (August 1991).

[4] O. K. Chopra, A. Sather and L. Y. Bush, Long-term embrittlement of cast duplex stainless steels in LWR systems. Semiannual Report, NUREG CR-4744, Vol. 4, No. 2, U.S. Nuclear Regulatory Commission, Washington, D.C., U.S.A. (June 1991).

[5] J. D. Landes, D. E. McCabe and H. A. Ernst, Elastic plastic methodology to establish R curves and sustainability criteria. Semiannual Report on EPRI Contract No. RP1238-2, July 1983 to December 1983, Westinghouse R&D Center (July 1984).

[6] W. A. Van Der Sluys, Toughness of ferritic piping steels. Final Report, EPRI NP-6264, Electric Power Research Institute, Palo Alto, California, U.S.A. (October 1988).

[7] J. R. Rice, A path-independent integral and the approximate analysis of strain concentration by notches and cracks. *J. appl. Mech.* **35**, 376–386 (1968).

[8] J. W. Hutchinson, Fundamentals of the phenomenological theory of nonlinear fracture mechanics. *J. appl. Mech.* **49**, 103–107 (1982).

[9] J. R. Rice and G. F. Rosengren, Plane strain deformation near a crack-tip in a power-law hardening material. *J. Mech. Phys. Solids* **16,** 1–12 (1968).
[10] J. W. Hutchinson, Singular behavior at the end of a tensile crack in a hardening material. *J. Mech. Phys. Solids* **16,** 13–31 (1968).
[11] P. C. Paris, H. Tada, A. Zahoor and H. Ernst, The theory of instability of the tearing mode of elastic–plastic crack growth. *ASTM STP* **668,** 5–36, American Society for Testing and Materials, Philadelphia, Pennsylvania, U.S.A. (1979).
[12] C. F. Shih and J. W. Hutchinson, Fully plastic solutions and large-scale yielding estimates for plane stress crack problems. *J. Engng Mater. Technol.* **98,** 289–295 (1976).
[13] V. Kumar, M. D. German and C. F. Shih, An engineering approach for elastic–plastic fracture analysis. EPRI/NP-1931, Electric Power Research Institute, Palo Alto, California, U.S.A. (1981).
[14] V. Kumar, M. German, W. Wilkening, W. Andrews, W. deLorenzi and D. Mowbray, Advances in elastic–plastic fracture analysis. EPRI/NP-3607, Electric Power Research Institute, Palo Alto, California, U.S.A. (1984).
[15] ADINA users manual. Report AE81-1, ADINA Engineering, Watertown, Massachusetts, U.S.A. (September 1981).
[16] P. Gilles and F. W. Brust, Approximate fracture methods for pipes—Part 1: theory. *Nuclear Engng Design* **127,** 1–27 (1992).
[17] F. Brust, S. Rahman and N. Ghadiali, Elastic–plastic analysis of small cracks in tubes. *J. Offshore Mech. Arctic Engng* **117,** 57–62 (1995); also available in the *Proc. Offshore Mechanics and Arctic Engineering*, Calgary, Canada (June 1992).
[18] *ABAQUS User's Guide and Manual.* Versions 4.6, 4.7 and 5.0, Hibbitt, Karlsson and Sorenson, Pawtucket, RI, U.S.A. (1993).
[19] F. W. Brust, P. Scott, S. Rahman, N. Ghadiali, T. Kilinski, R. Francini, C. Marschall, N. Miwia, P. Krishnaswamy and G. Wilkowski, Assessment of short through-wall circumferential cracks in pipes—experiments and analysis. NUREG/CR-6235, U.S. Nuclear Regulatory Commission, Washington, D.C., U.S.A. (1995).
[20] J. L. Sanders, Jr, Circumferential through-cracks in cylindrical shells under tension. *J. appl. Mech.* **49,** 103–107 (1982).
[21] J. L. Sanders, Jr, Circumferential through-crack in a cylindrical shell under combined bending and tension. *J. appl. Mech.* **50,** 221 (1983).
[22] R. Klecker, F. W. Brust and G. M. Wilkowski, NRC leak-before-break (LBB.NRC) analysis method for circumferentially through-wall cracked pipes under axial plus bending loads. NUREG/CR-4572, U.S. Nuclear Regulatory Commission, Washington, D.C., U.S.A. (1986).
[23] A. Zahoor, Closed form expressions for fracture mechanics analysis of cracked pipes. *J. Press. Vess. Technol.* **107,** 203–205 (May 1985).
[24] G. Wilkowski, F. Brust, R. Francini, N. Ghadiali, T. Kilinski, P. Krishnaswamy, M. Landow, C. Marschall, S. Rahman and P. Scott, Short cracks in piping and piping welds. Semiannual Reports, NUREG/CR-4599, BMI-2173, Vols 1–3, Nos 1 and 2, U.S. Nuclear Regulatory Commission, Washington, D.C., U.S.A. (1990–1994).
[25] S. Rahman, G. Wilkowski and F. Brust, Fracture analysis of full-scale pipe experiments on stainless steel flux welds. *Nuclear Engng Design* (1995) in press.
[26] S. Rahman, G. Wilkowski and F. Brust, Analysis of full-scale pipe fracture experiments on stainless steel flux welds. *Proc.* 1994 *ASME Pressure Vessels and Piping Division Conference*, Minneapolis, Minnesota, U.S.A. (June 1994).
[27] W. H. Press, B. P. Flannery, S. A. Teukolsky and W. T. Vetterling, *Numerical Recipes.* Cambridge University Press, New York, U.S.A. (1990).
[28] M. F. Kanninen, D. Broek, C. Marschall, E. Rybicki, S. Sampath, F. Simonen and G. Wilkowski, Mechanical fracture predictions for sensitized stainless steel piping with circumferential cracks. EPRI/NP-192, Electric Power Research Institute, Palo Alto, California, U.S.A. (1976).
[29] A. M. Hasofer and N. C. Lind, An exact and invariant first-order reliability format. *J. Engng Mech., ASCE* **100,** 111–121 (February 1974).
[30] B. Fiessler, H. J. Neumann and R. Rackwitz, Quadratic limit states in structural reliability. *J. Engng Mech., ASCE* **105,** 661–676 (1979).
[31] R. Rackwitz and B. Fiessler, Structural reliability under combined random load sequences. *Comput. Structures* **9,** 484–494 (1978).
[32] H. O. Madsen, S. Krenk and N. C. Lind, *Methods of Structural Safety.* Prentice-Hall, Englewood Cliffs, New Jersey (1986).
[33] M. Hohenbichler, New light and first- and second-order reliability methods. *Structural Safety* **4,** 267–284 (1987).
[34] K. Breitung, Asymptotic approximation for multinormal integrals. *J. Engng Mech., ASCE* **110,** 357–366 (March 1984).
[35] S. Rahman and M. Grigoriu, A Markov model for local and global damage indices in seismic analysis. NCEER-94-0003, National Center for Earthquake Engineering Research, State University of New York at Buffalo, Buffalo, New York, U.S.A. (1994).
[36] G. Fu and F. Moses, A sampling distribution for system reliability applications. *Proc. First IFIP WG 7.5 Working Conference on Reliability and Optimization of Structural Systems* (pp. 141–155), Aalborg, Denmark (May 1987).
[37] A. Harbitz, An efficient sampling method for probability of failure calculation. *Structural Safety* **3,** 109–115 (October 1986).
[38] A. Harbitz, Efficient and accurate probability of failure calculation by use of the importance sampling technique. *Proc. 4th Int. Conf. Applications of Statistics and Probability in Soil and Structural Engineering*, Florence, Italy (1983).
[39] Y. Ibrahim and S. Rahman, Reliability analysis of uncertain dynamic systems using importance sampling. *Proc. 6th Int. Conf. Applications of Statistics and Probability in Civil Engineering*, Mexico City, Mexico (1991).
[40] M. Hohenbichler, Improvement of second-order reliability estimates by importance sampling. *J. Engng Mech., ASCE* **114,** 2195–2199 (December 1988).
[41] R. E. Melchers, Efficient Monte Carlo probability integration. Report No. 7, Dept of Civil Engineering, Monash University, Australia (1984).
[42] P. Bjerager, Probability integration by directional simulation. *J. Engng Mech., ASCE* **114,** 1285–1302 (August 1988).
[43] I. Deak, Three digit accurate multiple normal probabilities. *Numerische Mathematik* **35,** 369–380 (1980).
[44] O. Ditlevson, R. Olesen and G. Mohr, Solution of a class of load combination problems by directional simulation. *Structural Safety* **4,** 95–109 (1986).
[45] R. Y. Rubinstein, *Simulation and the Monte Carlo Method.* John Wiley, New York, U.S.A. (1981).

[46] Report to the U.S. Nuclear Regulatory Commission Piping Review Committee, prepared by the Pipe Break Task Group, NUREG/CR-1061, Vol. 3., U.S. Nuclear Regulatory Commission, Washington, D.C., U.S.A. (November 1984).
[47] Published for public comment on Standard Review Plan, Section 3.6.3 LEAK-BEFORE-BREAK EVALUATION PROCEDURES, *Federal Register*, Vol. 52, pp. 32626–32633 (28 August 1987).
[48] S. Rahman, G. Wilkowski and N. Ghadiali, Pipe fracture evaluations for leak-rate detection: probabilistic models. *Proc. ASME Pressure Vessels and Piping Division Conference*, PVP-Vol. 266, Creep, Fatigue Evaluation, and Leak-Before-Break Assessment, Denver, Colorado, U.S.A. (July 1993).
[49] S. Rahman, G. Wilkowski and N. Ghadiali, Pipe fracture evaluations for leak-rate detection: applications to BWR and PWR piping. *Proc. ASME Pressure Vessels and Piping Division Conference*, PVP-Vol. 266, Creep, Fatigue Evaluation, and Lead-Before-Break Assessment, Denver, Colorado, U.S.A. (July 1993).
[50] 1989 Addenda ASME Boiler & Pressure Code—Section III, Article NB-3652.
[51] M. Rosenblatt, Remarks on a multivariate transformation. *Ann. Math. Statistics* **23**, 470–472 (1952).
[52] E. Parzen, *Modern Probability Theory and Its Applications*. John Wiley, New York, U.S.A. (1960).

(*Received* 11 *May* 1994)

APPENDIX A: COEFFICIENTS A_i, B_i AND C_{ij} FOR F-AND h_1-FUNCTIONS

A.1. *Coefficients* A_i *and* B_i

Let $\mathbf{A} = \{A_1, A_2, A_3\}^T$ and $\mathbf{B} = \{B_1, B_2, B_3, B_4\}^T$ be two vectors with the coefficients A_i and B_i as their components, respectively. **A** and **B** are given by:

$$\begin{aligned}\mathbf{A} &= \{0.006215 \quad 0.013304 \quad -0.018380\}^T \\ \mathbf{B} &= \{175.577 \quad 91.69105 \quad -5.53806 \quad 0.15116\}^T.\end{aligned} \tag{A1}$$

A.2. *Coefficients* C_{ij}

Let $\mathbf{C} = [C_{ij}]$, $i, j = 0$–3, be a matrix with the coefficients C_{ij} as its components. **C** is given by:

$R/t = 5$

$$\mathbf{C} = \begin{bmatrix} 3.74009 & 1.43304 & -0.10216 & 0.002297 \\ -0.19759 & -10.19727 & -0.45312 & 0.04989 \\ 36.42507 & 17.03413 & 3.36981 & -0.21056 \\ -70.4846 & -14.69269 & -2.90231 & 0.15165 \end{bmatrix} \tag{A2}$$

$R/t = 10$

$$\mathbf{C} = \begin{bmatrix} 3.39797 & 1.31474 & -0.07898 & 0.00287 \\ -3.07265 & 4.34242 & -2.48397 & 0.11476 \\ 131.7381 & -79.02833 & 16.18829 & -0.66912 \\ -234.6221 & 117.0509 & -20.30173 & 0.79506 \end{bmatrix} \tag{A3}$$

$R/t = 20$

$$\mathbf{C} = \begin{bmatrix} 4.07828 & -1.55095 & 0.67206 & -0.04420 \\ -18.21195 & 69.92277 & -18.41884 & 1.11308 \\ 357.4929 & -453.1582 & 108.0204 & -6.56651 \\ -602.7576 & 617.9074 & -144.9435 & 8.90222 \end{bmatrix}. \tag{A4}$$

APPENDIX B: FORM/SORM AND IMPORTANCE SAMPLING

B.1. *First- and Second-Order Reliability Methods (FORM/SORM)*

Consider a transformation $H: \mathbf{X} \to \mathbf{U}$, where $\mathbf{U} \in \mathbb{R}^N$ denotes an N-dimensional independent standard Gaussian random vector and $\mathbb{R}^N$ represents an N-dimensional real vector space. The transformation H is necessary if originally, the basic uncertainty vector **X** has an arbitrary joint distribution function $\mathbf{F}_{\mathbf{X}}(\mathbf{x})$. For example, when the Rosenblatt transformation [51] is used, the explicit form of above mapping from original **x** space to **u** space becomes

$$H: \begin{cases} u_1 = \Phi^{-1}[F_1(x_1)] \\ u_2 = \Phi^{-1}[F_2(x_2|x_1)] \\ \quad\vdots \quad\quad \vdots \\ u_n = \Phi^{-1}[F_n(x_n|x_1, x_2, \ldots, x_{n-1})], \end{cases} \tag{B1}$$

in which $F_i(x_i|x_1, x_2, \ldots, x_{i-1})$ is the cumulative distribution function of component X_i conditional on $X_1 = x_1$, $X_2 = x_2, \ldots, X_{i-1} = x_{i-1}$ and $\Phi(\cdot)$ is the cumulative distribution function of a standard Gaussian random variable. $F_i(x_i|x_1, x_2, \ldots, x_{i-1})$ can be obtained from

$$F_i(x_i|x_1, x_2, \ldots, x_{i-1}) = \frac{\int_{-\infty}^{x_i} f_{1,2,\ldots,i}(x_1, x_2, \ldots, x_{i-1}, s)\,\mathrm{d}s}{f_{1,2,\ldots,i-1}(x_1, x_2, \ldots, x_{i-1})}, \tag{B2}$$

where $f_{1,2,\ldots,i-1}(x_1, x_2, \ldots, x_{i-1})$ is the joint probability density function of $\{X_1, X_2, \ldots, X_{i-1}\}^T$. The inverse transformation can be obtained in a stepwise manner as

$$H^{-1}: \begin{cases} x_1 = F_1^{-1}[\Phi(u_1)] \\ x_2 = F_2^{-1}[\Phi(u_2)|x_1] \\ \vdots \quad \vdots \\ x_n = F_n^{-1}[\Phi(u_n)|x_1, x_2, \ldots, x_{n-1}], \end{cases} \tag{B3}$$

which when substituted into eq. (19) yields

$$\begin{aligned} P_F &= \Pr[g_U(\mathbf{U}) < (0)] \\ &= \int_{g_U(\mathbf{U})<0} \phi(\mathbf{u})\, d\mathbf{u}, \end{aligned} \tag{B4}$$

where $\phi(\mathbf{u})$ is the standard multivariate Gaussian probability density function defined as

$$\phi(\mathbf{u}) = (2\pi)^{-N/2} \exp(-\tfrac{1}{2}\mathbf{u}^T\mathbf{u}) \tag{B5}$$

and $g_U(\mathbf{u})$ is the new limit state surface in the Gaussian image $\mathbf{u}$ of the original space $\mathbf{x}$. Note that eq. (B4) represents the same N-dimensional integral of eq. (19) in a different space than the original space due to the change of variables described earlier. The integral is still difficult to compute unless some approximations are sought for the domain of the integral.

B.1.1. *First-Order Reliability Method (FORM).* Consider a tangential linearization at the point $\mathbf{u}^*$ of the limit state surface $g_U(\mathbf{u}) = 0$ which is given by

$$g_L(\mathbf{u}) = \boldsymbol{\alpha}^T(\mathbf{u} - \mathbf{u}^*) = 0, \tag{B6}$$

where $\mathbf{u}^*$ is the closest point (known as the design point, beta point, etc.) of $g_U(\mathbf{u}) = 0$ to the origin of $\mathbf{u}$ space, and $\boldsymbol{\alpha} \in \mathbb{R}^N$ is the vector of direction cosines. $\boldsymbol{\alpha}$ can be obtained from

$$\boldsymbol{\alpha} = \frac{\nabla g_U(\mathbf{u}^*)}{\|\nabla g_U(\mathbf{u}^*)\|}, \tag{B7}$$

in which

$$\nabla = \left\{ \frac{\partial}{\partial u_1} \quad \frac{\partial}{\partial u_2} \quad \cdots \quad \frac{\partial}{\partial u_N} \right\}^T, \tag{B8}$$

with $\nabla g_U(\mathbf{u}^*)$ as the gradient of scalar field $g_U(\mathbf{u})$ at $\mathbf{u}^*$, and

$$\|\nabla g_U(\mathbf{u}^*)\| = \sqrt{\sum_{i=1}^{N} \left| \frac{\partial g_U}{\partial u_i}(\mathbf{u}^*) \right|^2} \tag{B9}$$

is the Euclidean L_2-norm of an N-dimensional vector $\nabla g_U(\mathbf{u}^*)$. The distance β_{HL} of this point $\mathbf{u}^*$ to the origin of $\mathbf{u}$ space is referred to as the Hasofer–Lind Reliability Index [29]. β_{HL} can be obtained from a nonlinear optimization scheme which can be mathematically formulated as

$$\begin{aligned} \beta_{HL} &= \inf_{g_U(\mathbf{u})=0} \|\mathbf{u}\| \\ &= \|\mathbf{u}^*\| \\ &= \boldsymbol{\alpha}^T\mathbf{u}^*, \end{aligned} \tag{B10}$$

which requires determination of the design point $\mathbf{u}^*$. When the linear approximation of the limit state in eq. (B6) is substituted into eq. (B4), the estimate of P_F by FORM becomes [31]

$$\begin{aligned} P_{F,1} &= \int_{\boldsymbol{\alpha}^T(\mathbf{u}-\mathbf{u}^*)<0} \phi(\mathbf{u})\, d\mathbf{u} \\ &= \int_{\boldsymbol{\alpha}^T\mathbf{u}-\beta_{HL}<0} \phi(\mathbf{u})\, d\mathbf{u} \\ &= \Phi(-\beta_{HL}). \end{aligned} \tag{B11}$$

B.1.2. *Second-Order Reliability Method (SORM).* Consider a suitable rotational transformation from $\mathbf{u}$ space to $\mathbf{v}$ space so that the mapped design point $\mathbf{v}^*$ in $\mathbf{v}$ space has the coordinates $(0, 0, \ldots, -\beta_{HL})$. Suppose, the transformed vector $\mathbf{v} = \{v_1, v_2, \ldots, v_N\} = \{\mathbf{v}_r, v_N\}^T$ where $\mathbf{v}_r = \{v_1, v_2, \ldots, v_{N-1}\}$ is the reduced vector and $v_N = h_V(\mathbf{v}_r)$ which is the root of the mapped limit state surface $g_V(\mathbf{v}_r, v_N) = 0$ in $\mathbf{v}$ space. In this way, the limit state surface $g_V(\mathbf{v}) = g_V(\mathbf{v}_r, v_N) = 0$ can be alternatively represented by $v_N = h_V(\mathbf{v}_r)$ in the $\mathbf{v}$ space. Consider now a second-order approximation $g_Q(\mathbf{v}) = 0$ or rather an approximation $v_N = h_V(\mathbf{v}_r)$ in the $\mathbf{v}$ space. Consider now a second-order approximation $g_Q(\mathbf{v}) = 0$ or rather an approximation $v_N = h_Q(\mathbf{v}_r)$ to $v_N = h_V(\mathbf{v}_r)$ of the limit state surface. If the quadratic approximant is of special form, e.g. the rotational hyperparaboloid, it can be shown that

$$h_Q(\mathbf{v}_r) = -\beta_{HL} + \frac{1}{2}\sum_{i=1}^{N-1} \kappa_i v_i^2 \tag{B12}$$

where κ_i is the ith principal curvature of the limit state surface at the design point. The above quadratic is equivalent to the actual $v_N = h_V(\mathbf{v}_r)$ in the sense that

$$h_Q(\mathbf{v}_r^*) = h_V(\mathbf{v}_r^*) \tag{B13}$$

$$\frac{\partial h_Q}{\partial v_i}(\mathbf{v}_r^*) = \frac{\partial h_V}{\partial v_i}(\mathbf{v}_r^*) \tag{B14}$$

$$\frac{\partial^2 h_Q}{\partial v_i \partial v_j}(\mathbf{v}_r^*) = \frac{\partial^2 h_V}{\partial v_i \partial v_j}(\mathbf{v}_r^*), \tag{B15}$$

for $i, j = 1, 2, \ldots, N-1$. When the actual limit state surface is approximated by the hyperparaboloid in eq. (B12), the estimate of P_F by SORM becomes [34]

$$P_{F,2} \simeq \Phi(-\beta_{HL}) \prod_{i=1}^{N-1} (1 - \kappa_i \beta_{HL})^{-1/2} \tag{B16}$$

which is asymptotically exact when β_{HL} approaches infinity. An improvement over above probability estimate has also been proposed by Hohenbichler [33] which gives

$$P_{F,2} \simeq \Phi(-\beta_{HL}) \prod_{i=1}^{N-1} [1 - \kappa_i \Psi(-\beta_{HL})]^{-1/2}, \tag{B17}$$

where

$$\Psi(-\beta_{HL}) = \frac{\phi(-\beta_{HL})}{\Phi(-\beta_{HL})}. \tag{B18}$$

Note that when β_{HL} approaches infinity, $\Psi(\beta_{HL})$ approaches β_{HL} and eq. (B17) degenerates to eq. (B16) as expected.

B.2. *Importance sampling*

Consider eq. (B4), which can be rewritten in the form

$$\begin{aligned} P_F &= \Pr[g_{app}(\mathbf{U}) < 0] \times \frac{\Pr[g_U(\mathbf{U}) < 0]}{\Pr[g_{app}(\mathbf{U}) < 0]} \\ &= \Pr[g_{app}(\mathbf{U} < 0] \times C_F \end{aligned} \tag{B19}$$

where $g_{app}(\mathbf{U})$ is either the linear or quadratic approximation of the limit state surface $g_U(\mathbf{U})$ and $C_F = \Pr[g_U(U) < 0] / \Pr[g_{app}(\mathbf{U}) < 0]$ is the correction factor improving the reliability estimate by $g_{app}(\mathbf{U})$. When the quadratic approximation in eq. (B12) is used, C_F can be approximated by simulation with importance sampling. According to Hohenbichler [40], it is given by

$$C_F \simeq \frac{1}{N_{IS}} \sum_{j=1}^{N_{IS}} C_{F,j}, \tag{B20}$$

in which

$$C_{F,j} = \frac{\Phi(h_Q(\mathbf{w}_j))}{\Phi(\beta_{HL})} \exp\left[-\frac{1}{2} \Psi(\beta_{HL}) \sum_{k=1}^{N-1} \kappa_k w_{k,j}^2 \right], \tag{B21}$$

where $\mathbf{w}_j = \{w_{1,j}, w_{2,j}, \ldots, w_{N-1,j}\}^T$ is the jth realization of the independent Gaussian random vector $\mathbf{W} \in \mathbb{R}^{N-1}$ with mean $E[W_i]$ and variance $\mathrm{Var}[W_i]$ of ith component given by

$$E[W_i] = 0 \tag{B22}$$

$$\mathrm{Var}[W_i] = \frac{1}{[1 - \Psi(-\beta_{HL})]} \tag{B23}$$

and N_{IS} is the total number of samples for this simulation. Thus, the estimates of $P_{F,IS}$ by simulation with importance sampling become

$$P_{F,IS} \simeq \Phi(-\beta_{HL}) \prod_{i=1}^{N-1} [1 - \kappa_i \Psi(-\beta_{HL})]^{-1/2} \frac{1}{N_{IS}} \sum_{j=1}^{N_{IS}} \frac{\Phi(h_Q(\mathbf{w}_j))}{\Phi(\beta_{HL})} \exp\left[-\frac{1}{2} \Psi(\beta_{HL}) \sum_{k=1}^{N-1} \kappa_k w_{k,j}^2 \right]. \tag{B24}$$

APPENDIX C: SAMPLE GENERATION OF RANDOM VECTOR

A simple method is presented for generating samples of N-dimensional generic random vector $\mathbf{X} = \{X_1, X_2, \ldots, X_N\}^T$ with arbitrary joint distribution function $F_{\mathbf{X}}(\mathbf{x})$. The vector $\mathbf{X}$ may have independent and correlated components.

C.1. *Independent random parameters*

Consider a random component X_i with the cumulative probability distribution function $F_{X_i}(x_i)$. Let Z_i be a random variable uniformly distributed in the interval [0, 1]. It has the distribution function $F_{Z_i}(z_i) = z_i$. For a probability preserving transformation with the distribution functions of X_i and Z_i being equal, the realization x_i of random variable X_i can be obtained as

$$x_i = F_{X_i}^{-1}(z_i). \tag{C1}$$

A two-step simulation technique can be developed based on this transformation. First, a sample z_i of Z_i is generated, e.g. by using a standard random number generator available in any computer. Second, a sample of X_i can be obtained from eq. (C1). Thus, by generating independent samples of Z_i, one can obtain from eq. (C1) independent samples of X_i.

Alternative simulation techniques are available and can be found in ref. [45]. They are based on characteristics of various probability distributions.

C.2. *Dependent random parameters*

Consider an N-dimensional random vector $\mathbf{X}$ with a generic joint distribution function $F_{\mathbf{X}}(\mathbf{x})$. A three-phase method can be applied to generate samples $\mathbf{x}$ of $\mathbf{X}$. First, generate N independent uniformly distributed samples $z_1, z_2, \ldots, z_N$ in the interval [0, 1]. Second, map each of these samples into a sample u_i of a standard Gaussian random variable U_i. For example, u_i can be obtained from $u_i = \Phi^{-1}(z_i)$, $i = 1, 2, \ldots, N$ where $\Phi(\cdot)$ is the cumulative distribution function of a

standard Gaussian random variable. Third, use the Rosenblatt transformation described in Appendix B to map the sample of the standard Gaussian vector $\mathbf{U} = \{U_1, U_2, \ldots, U_N\}^T$ into corresponding samples of $\mathbf{X} = \{X_1, X_2, \ldots, X_N\}^T$. For special cases, when the random vector $\mathbf{X}$ is correlated Gaussian or correlated lognormal, the Rosenblatt transformation can be sidestepped by using Cholesky decomposition of the covariance matrix. They are described below.

C.2.1. *Multivariate normal distribution.* Let $\mathbf{X}$ be an N-dimensional normal vector with mean vector $\boldsymbol{\mu}$ and covariance matrix $\boldsymbol{\Sigma}$. Consider a linear transformation of the form

$$\mathbf{X} = \mathbf{D} + \mathbf{Q}\mathbf{U}, \tag{C2}$$

where $\mathbf{U}$ is a standard Gaussian random vector, $\mathbf{D}$ is an N-dimensional transformation vector and $\mathbf{Q}$ is an $N \times N$ transformation matrix. Applying a linear expectation operator on $\mathbf{X}$ and $(\mathbf{X} - \boldsymbol{\mu})(\mathbf{X} - \boldsymbol{\mu})^T$, it is elementary to show that

$$\begin{aligned} \boldsymbol{\mu} &= \mathbf{D} \\ \boldsymbol{\Sigma} &= \mathbf{Q}\mathbf{Q}^T. \end{aligned} \tag{C3}$$

From eq. (C3), $\mathbf{D}$ is equal to $\boldsymbol{\mu}$ and $\mathbf{Q}$ is a lower triangular matrix representing Cholesky decomposition of $\boldsymbol{\Sigma}$. Standard methods of linear algebra can be used to determine $\mathbf{Q}$ [27].

C.2.2. *Multivariate lognormal distribution.* Let $\mathbf{X}$ be an N-dimensional lognormal vector with mean vector $\boldsymbol{\mu}$ and covariance matrix $\boldsymbol{\Sigma}$. Suppose that $\mathbf{Y}$ is an N-dimensional Gaussian random vector with component $Y_i = \ln X_i$, $i = 1, 2, \ldots, N$. Let $\boldsymbol{\mu}_Y$ and $\boldsymbol{\Sigma}_Y$ denote the mean and covariance matrix of $\mathbf{Y}$. From moment generating function of $\mathbf{Y}$, it can be shown that the mean and the covariance properties of $\mathbf{Y}$ are [52]

$$\mu_{Y,i} = \ln \mu_i - \tfrac{1}{2} \ln(1 + V_i^2) \tag{C4}$$

and

$$\begin{aligned} \Sigma_{Y,ii} &= \ln(1 + V_i^2) \\ \Sigma_{Y,ij} &= \ln[1 + \rho_{ij} V_i V_j], \end{aligned} \tag{C5}$$

where μ_i is the ith component of $\boldsymbol{\mu}$, $\mu_{Y,i}$ is the ith component of $\boldsymbol{\mu}_Y$, Σ_{ij} is the (i, j)th element of $\boldsymbol{\Sigma}$, $\Sigma_{Y,ij}$ is the (i, j)th element of $\boldsymbol{\Sigma}_Y$, $V_i = \sqrt{\Sigma_{ii}}/\mu_i$ is the coefficient of variation of X_i and $\rho_{ij} = \Sigma_{ij}/(\sqrt{\Sigma_{ii}}\sqrt{\Sigma_{jj}})$ is the correlation coefficient between random variables X_i and X_j. Following calculations of statistics of Gaussian vector $\mathbf{Y}$ from eqs (C4) and (C5), the same type of linear mapping described in Section C.2.1 [e.g. eq. (C2)] can be applied for transforming $\mathbf{Y}$ into standard Gaussian random vector $\mathbf{U}$.